The Hydrodynamic Structure of Detonations

Matei I. Radulescu[1], Gary J. Sharpe[2] and Chung K. Law[1]
[1]Princeton University, Princeton, NJ, USA
[2]University of Birmingham, Birmingham, U.K.

Corresponding author, Matei I Radulescu: mradules@princeton.edu

Abstract

Most detonations are unstable, their reaction zones are turbulent and their structure departs significantly from the idealized one-dimensional Zeldovich-Von Neumann-Doering model (ZND). Recent numerical studies (Ng et al., 2005) further demonstrated that detonation waves are chaotic, following the Feigenbaum bifurcation route. Parameters corresponding to typical reacting systems fall in the chaotic regime. Since a deterministic theory for such detonations is not possible, the present study considers a stochastic one-dimensional treatment and model for such detonation waves. Real and numerical experiments are used to verify whether the space and time-averaged structure of detonations can be described by a generalized probabilistic one-dimensional ZND theory, with a statistically determined sonic surface, dictated by the competition between the various global chemical, mechanical and thermal relaxation processes.

---

1. Introduction

Research in the past 50 years has demonstrated that most self-sustaining detonations in gaseous explosive mixtures are unstable and have a three-dimensional non-steady cellular structure. An example of the simpler two-dimensional frontal cellular structure obtained in a thin channel (Radulescu et al., 2005), as to eliminate most of the three-dimensional effects, is shown in Figure 1, along with an explanatory sketch. The two-dimensional cell boundaries are formed by the intersection of transverse shock waves with the leading shock front. These shock interactions are triple-shock Mach intersections. Shear layers and transverse shocks extend from the cell boundaries into the reaction zone behind the leading shocks. The transverse shocks sweep laterally across the leading shock surface and collide with each other. They also interact and sometimes couple with the reaction layers (e.g. Figure 1). These shock reflections also cause the leading shock front to pulsate in the direction of propagation and alternate between strong Mach stems and weaker incident shocks. Between transverse wave collisions, the velocity of the leading shock generally fluctuates between approximately 1.6 and 0.75 times the average velocity. Due to this very large variation in leading shock strengths, the reaction rates behind the strong Mach stems (central part of the front in Fig. 1) can be as much as 7 to 8 orders of magnitude larger than the gas shocked by the weaker incident shocks (top and bottom segments in Fig. 1). These differences are the greatest in systems with large chemical activation energies, due to the exponential dependence of reaction rates on local shock temperature. For gases with high activation energies, as is the case for the methane-oxygen mixture shown in Fig. 1, and for most fuel-air mixtures of practical interest (e.g., hydrocarbon and hydrogen mixtures), the gases shocked by the weaker incident shocks remain un-reacted as unburned pockets (Austin et al., 2005, Radulescu et al. 2005) and are subsequently burned by turbulent diffusional mechanisms at small scales (Radulescu et al. 2005), favored by Kelvin-Helmholtz instabilities at shear layers

and Taylor instabilities when transverse shocks interact with density interfaces separating reacted and un-reacted gases. In spite of these complex phenomena, the average velocity of the detonation wave is in general very close to the Chapman-Jouguet value for mixtures well within the detonability limits.

The effect of instability on detonation dynamics has recently been investigated by Ng et al. (2005) in the idealized framework of one-dimensional inviscid detonation waves. Taking the sensitivity of the reaction rates (the reduced activation energy) as governing parameter in their study, Ng et al. have showed that detonation pulsations are chaotic, following the classic route to chaos involving period doubling bifurcations governed by the Feigenbaum constant. Their results have been recently verified with much higher precision by Henrick et al. (2005). These remarkable discoveries show that detonation waves share the same properties as many other non-linear systems that transit to chaos and turbulence, including hydrodynamic turbulence (Landau & Lifshitz, 2003). What is more remarkable and instructive is that instability first occurs at a chemical activation energy of ~26 and become chaotic with very complex dynamics at ~28, whether this parameter in typical detonation waves is approximately double, suggesting that most detonations operate in a "fully-developed" chaotic regime. These findings suggest that a theoretical deterministic model for detonations, other than Direct Numerical Simulation (DNS) of the Navier-Stokes equations, is impossible and futile. A probabilistic approach to detonations thus appears more worthwhile.

In spite of the chaotic property, it is interesting to note that the detonation structure is organized in a three-dimensional cellular structures of a fixed outer dimension, the cell width λ, but with a continuous range of fluctuations at smaller scales, without any apparent discontinuity. An example of the cellular structure formed by triple point imprints on a plate covered with soot is shown in Figure 2 for the methane-oxygen system considered above, taken from (Austin, 2003). As can be seen, there is a continuous range of spacings, with a maximum value on the order of 100 mm for this mixture. The intermittent cellular structure of such highly unstable detonations should not be a feature to dissuade an attempt at a probabilistic model. Instead, the organization into a cellular structure can be viewed as a turbulent intermittency effect, persisting in a fully-developed turbulence regime, analoguous to vortex filaments formation in incompressible turbulence (Frisch, 1995). Furthermore, since a maximum cell width λ exists in a detonation wave, this length scale can be considered as an integral scale in a turbulent regime (Radulescu et al., 2005). Previous empirical correlations also used the cell width λ for predicting the dynamic detonation parameters (Lee, 1984) (e.g., detonation limits, critical initiation energy, critical tube diameter, etc…) with good success. Alternatively, the use of the idealized ZND structure for the determination of these dynamic parameters usually gives unacceptable results (e.g., Radulescu & Lee, 2002). Thus, there is good empirical evidence that a global treatment of the turbulent reaction zone structure, characterized by an outer scale such as the cell size λ, is more satisfactory than a laminar model based on a one-dimensional reaction zone structure.

A stochastic description of the detonation wave structure was attempted in the past in a number of studies (Voitsekhovskii et al., 1963, White, 1961, Strehlow, 1971, Panton, 1971, Rybanin, 1966, Nikolaev & Zak, 1989), where the equations of motion were Reynolds averaged, and their qualitative properties compared with Chapman-Jouguet (CJ) theory for laminar flow. These models were not applied to capture nor predict any features of cellular detonations, nor was the structure observed experimentally interpreted in terms of the model equations, since accurate measurements in the reaction zone were not available at the time. In the present study,

numerical simulations and experimental results are used to investigate the statistical properties of gaseous detonations, focusing on the highly unstable detonations. Of particular interest is the comparison of results obtained from cellular detonations with the predictions obtained from classical CJ theory, which predicts the thermodynamic states bounding the wave, treating the wave as a reacting discontinuity.

The CJ theory rests on the hypothesis that the burned gases are in chemical equilibrium and flow at sonic velocity relative to the front. This sonic surface in the burned products acts as an information boundary and separates the steady detonation wave structure from the trailing unsteady expansions, which cannot penetrate into the reaction zone. The validity of the CJ hypothesis may not be valid in real experiments, since large fluctuations persist behind the wave. Furthermore, a sonic surface seems difficult to define in an unsteady flow with large fluctuations. In the present study, we investigate in greater detail the effect of such fluctuations on the state behind the wave and the location of a statistically determined sonic surface.

Usually, the CJ theory cannot be verified experimentally with adequate accuracy. This is due primarily to the dependence of detonations on boundary conditions, such tube losses, which are not easily accounted in the models. Furthermore, the thermodynamic state behind the wave is difficult to measure with high accuracy, since boundary effects and strong fluctuations render experimental measurements very difficult. An excellent review of experimental results obtained for the thermodynamic state in the detonation products and comparison with theory can be found in (Fickett & Davis, 1979). The consensus reached is that in general the wave velocity is typically within 2% of the ideal value. The end state behind the wave is found to lie somewhat lower than the ideal CJ point on the burned equilibrium Hugoniot, i.e. on the weak branch. A clear verification or explanation for these observations, or alternatively a validation of CJ theory in real detonations, is still lacking. The present paper addresses these shortcomings and investigates the structure of turbulent detonation waves in a stochastic framework, with a particular emphasis on the location of the sonic surface in cellular detonations and the processes that govern its location. The first section of the paper reviews previous efforts at estimating the reaction zone thickness and measuring the location of the sonic surface in real detonations. The second section describes the results of numerical experiments of unstable detonations in two dimensions and compares the results with physical experiments. The effect of relaxation processes on the global thickness of the wave and location of the averaged sonic surface are further investigated for weakly unstable detonation, for which higher numerical resolutions can be obtained. The last section discusses the formulation of a stochastic model for detonation waves and the effect of fluctuations on the global structure.

2. Previous estimates of the hydrodynamic thickness of detonation waves

Soloukhin was the first to attempt to estimate an appropriate thickness of cellular detonations by taking into consideration the non-steady gasdynamic processes operating behind the pulsating leading shock front (Soloukhin, 1966, 1969, Lee et al., 1969). He introduced the terminology “hydrodynamic thickness” to emphasize the effect of the non-steady gasdynamic expansion processes on the reaction rates. Subsequent studies by Lundstrom & Oppenheim (1969), Strehlow (1971) and Edwards et al. (1976) used strong blast wave theory to model the decaying lead shock front and compute the chemical reactions in the expansion flow behind the decaying blasts. These early attempts demonstrated qualitatively that the gasdynamic expansions lengthen the induction times by several orders of magnitude behind the decaying shocks, leading to global reaction lengths much longer than obtained behind a steadily moving shock, as

predicted by the steady ZND model. The estimates were found to be highly dependent on the chemical rate sensitivity. For more unstable detonations, the induction delay times were estimated to reach infinite values for most of the gas processed behind the decaying shock fronts (Lundstrom & Oppenheim, 1969, Austin et al. 2005, Radulescu et al. 2005), although in reality, they reacted much more rapidly. These observations lead to the conclusion that multi-dimensional effects, such transverse wave interactions and turbulence play an integral part in the ignition mechanism, and the a priori knowledge of the leading shock front history is insufficient to estimate the global reaction rates. Consequently, it appears that a more realistic estimate for the hydrodynamic thickness based on the chemical relaxation process would require a more detailed description of the turbulent reaction zone itself. In view of the complicated turbulent structure of the wave, this would be a formidable task.

However, irrespective of the highly transient three-dimensional turbulent structure of "real detonations", their propagation speed is found to be constant on average, and generally very close to the theoretical value determined from the solution of the steady one-dimensional conservation equations based on the Chapman-Jouguet criterion of sonic flow at chemical equilibration. The implication of these observations is that CJ theory should give a good first order approximation for the average fluid states bounding the mean detonation structure. It is thus not unreasonable to expect that the rear of the wave must hence be described, at least in an average sense, by a rear limiting characteristic surface propagating at $u^* + c^*$, which has to equal the detonation wave velocity D (i.e. $D = u^* + c^*$) and separates the statistically average detonation structure from any trailing unsteady expansion waves, see Figure 3. Because any unsteady expansion, such the Taylor wave behind a detonation propagating in a closed end tube (Taylor 1950), cannot penetrate into the detonation wave structure and hence ensures that the detonation wave is self-sustained at a mean constant speed, the distance between the shock and the limiting characteristic surface should be the suitable measure for the detonation wave thickness. This limiting characteristic is a sonic plane in the detonation frame of reference. Clearly, if u' represents the particle velocity in the detonation frame of reference, i.e. $u' = D - u$, than along this limiting characteristic, the flow velocity u'^* is sonic (i.e. $u'^* = c^*$). A schematic for the limiting characteristic separating the steady detonation wave structure from the following expansion waves is shown in Figure 3. The dynamics of the instantaneous limiting characteristic surface, as it varies with time, was recently studied numerically by Kasimov & Stewart (2004) for one-dimensional pulsating detonation waves. For a turbulent multi-dimensional detonation, however, tracking the local dynamics of a characteristic surface would be extremely more difficult. Instead, we are interested in its mean location, situated at some distance behind the mean detonation front, which henceforth defines the hydrodynamic thickness.

Experimentally, the first attempt to measure the hydrodynamic thickness in real cellular detonations was made by Vasil'ev et al. (1972). The method used by Vasil'ev consisted of placing a small blunt body protrusion in the path of the detonation wave. When the velocity of the local fluid passing over the obstacle is supersonic, as it is immediately behind the leading shock front of the detonation wave, a bow shock wave appears and remains attached to the body as long as the flow remains supersonic. When the flow becomes subsonic in the obstacle frame of reference (i.e. the laboratory frame of reference), the bow shock detaches from the obstacle and propagates upstream. Observation of the attached bow shock hence permits to determine the location behind the detonation front where the flow is sonic in the laboratory frame of reference. It is very important to note that the location of sonic flow in the laboratory coordinates, i.e. in the frame of reference of the blunt body, does not correspond to the location of sonic surface in the

detonation frame, which is the locus of the limiting characteristic surface. For example, since the velocity in the laboratory frame is given by $u = D - u'$, then at the real sonic plane, the Mach number of the flow in the laboratory coordinates is $M^*_{lab} \equiv u^*/c^* = D/c^* - 1$. It can easily be verified that M^*_{lab} is always less than unity at the real sonic plane. For example, if one assumes a strong detonation wave, $M^*_{lab} = 1/\gamma$ at the real sonic plane. It follows that Vasil'ev's technique always underestimates the true location of the sonic surface. Nevertheless, since in general γ is close to unity in the burnt products ($\gamma \cong 1.1$), his technique can be used as a first order lower bound estimate for the location of the limiting characteristic. A more recent attempt using the same technique was performed by Weber & Oliver (2004), who also used arrays of obstacles to obtain a more spatially resolved location of the sonic surface. The measurements for the location of the laboratory sonic plane of Vasil'ev and Weber and Olivier varied between 0.5 and 3 detonation cell widths λ, with the upper bound corresponding to conditions removed from marginality where the tube diameter is larger than a few characteristic cell sizes λ. Since the cell size λ is typically one to two orders of magnitude larger (Gavrikov et al. 2000) than the reaction zone thickness of laminar detonations, it follows that the hydrodynamic thickness is significantly larger than the laminar reaction zone width.

According to the one-dimensional inviscid theory, the sonic surface provides the matching point between the steady reaction zone structure and the unsteady expansions trailing behind the detonation wave. This surface would hence mark a first order discontinuity in the thermodynamic variables, i.e. a discontinuity in slope. Edwards et al. (1976) attempted to identify such discontinuous behavior from pressure measurements of the reaction zone. However, they encountered difficulties due to the large pressure fluctuations in the reaction zone. They nevertheless estimated the location of the onset of the Taylor wave at approximately 4 to 10 λ downstream of the leading front. They also found that this length scale also corresponded to the decay of the pressure oscillations to a negligible intensity and the approach of the mean pressure profiles to the ideal equilibrium CJ values. Since they noted that in general the global chemical reaction length (typically a fraction of a cell width λ) is much shorter than the measured hydrodynamic thickness, they suggested that the appearance of the sonic plane could be linked to the equilibration of the mechanical fluctuations and dissipation of the turbulent energy into mean kinetic and internal energy. Edwards' estimates for the location of the sonic surface were higher than the measurements of Vasil'ev and Weber & Olivier, consistent with the fact the latter were only a lower bound estimate for the location of the real CJ surface. However, they agreed well with the earlier measurements of Soloukhin for the onset of the Taylor expansion, whose results also reveal that the limiting characteristic is situated approximately at 4λ downstream of the leading front (Soloukhin, 1966)

The conclusion that can be reached is that a proper characterization of the location of the sonic surface in real detonations could hence provide the details of the mechanical and thermal equilibration process, which lead to the lengthening of the detonation structure.

3. Numerical set - up

The computations were performed in two dimensions using the μCobra code, described in (Sharpe, 2001). We are assuming we are dealing with a perfect binary gas with equal specific heats and molecular weights. The governing equations are the Navier-Stokes equations for reacting gas (Williams, 1985)

$$\rho_t + \nabla \cdot (\rho U) = 0 \tag{3.1}$$

$$(\rho U)_t + \nabla \cdot (\rho UU + p) = -\nabla \cdot \sigma_{viscous} \tag{3.2}$$

$$E_t + \nabla \cdot ((E+p)U) = -\nabla \cdot (k_{cond} \nabla T) - \nabla \cdot (U \cdot \sigma_{viscous}) - Q\nabla \cdot (\rho D \nabla \alpha) \tag{3.3}$$

$$(\rho\alpha)_t + \nabla \cdot (\rho U \alpha) = \dot{w} + \nabla \cdot (\rho D_{diff} \nabla \alpha) \tag{3.4}$$

where E represents the total energy (internal, kinetic and chemical)

$$E \equiv \frac{p}{\gamma - 1} + \frac{1}{2}\rho |U|^2 + \rho\alpha Q \tag{3.5}$$

and α is the reaction progress variable, taken as the mass fraction of reactant and Q is the available chemical energy. For simplicity, we are assuming the reactions proceed via a single step reaction given by Arrhenius kinetics:

$$\dot{w} = -k\rho\alpha e^{-\frac{Ea}{RT}} \tag{3.6}$$

where E_a is the activation energy and k a constant, which sets the unit time scale in the computations.

The viscous terms on the right hand sides are the usual transport terms. These terms, representing higher derivatives are very difficult to compute accurately due to the very high Reynolds numbers encountered in practice, typically 10^6-10^7 based on the cell size λ as a characteristic scale. For this reason, the viscous and diffusive terms only operate at the very small scales, near the sharp gradients appearing in the solution, and are very difficult to capture computationally. We are not solving these terms explicitly, with the clear knowledge that the solutions so-obtained are neither the true solutions of the reacting Euler equations, neither the solutions of the true Navier-Stokes equations, but involve numerical dissipation as the small scale limit.

The thermo-chemical parameters were chosen to represent two distinctive cases of cell regularity. The first parameters were chosen to represent methane-oxygen detonations (Radulescu et al. 2005), for which we also present the results of real experiments below. The effective activation energy, heat release and isentropic exponent are taken as $E_a/RT_{VN} = 11$, $Q/RT_{VN} = 7.5$ and $\gamma = 1.24$, corresponding to $E_a/RT_o = 63.7$ and $Q/RT_o = 43$; where the subscripts "o" and "VN" refer to the initial state and the Von Neumann shock state of the ZND model, respectively. Due to the highly unstable nature of this front, the maximum resolution in the adaptive mesh refinement code was set to 128 points per half reaction length $\Delta_{1/2}$ of the steady wave (i.e. the point where 50% of the energy is released). The second computation was performed for a generic weakly unstable detonation, with parameters $E_a/RT_{VN} = 5.6$, $Q/RT_{VN} = 10.4$, $\gamma = 1.2$ (corresponding to $E_a/RT_O = 27$, $Q/RT_O = 50$), characterized by a single one-dimensional unstable mode in the transition to chaos study of (Ng et al., 2005). Due to the much weaker level of instability, a resolution of 32 points per $\Delta_{1/2}$ was used. In both cases, the detonation was initiated by a strong blast wave, obtained by the deposition of a large amount of energy in a few grid cells near the origin. The front then decayed towards a self-sustained detonation wave. The computational domain extended to the back wall where the detonation was initiated and solved explicitly the unsteady Taylor expansion wave behind the detonation front. To save on the computational price, the computational domain width was set to permit a single mode detonation with a single triple point, such that the integral scale of the detonation dynamics corresponds to the physical domain width. This corresponded to setting the height of the 2-

dimensional channel to $6\Delta_{1/2}$ and $10\Delta_{1/2}$ for the highly unstable and weakly unstable detonations, respectively.

4. Numerical results for high activation energy detonations

The wave was initiated with a one-dimensional blast wave profile, which was given a perturbation to generate the cellular structure. Figure 4 shows the numerical "open shutter" photograph, analogous to the experimental records obtained by the time-integrated luminosity technique; instead we are using the intermittent zones of chemical energy release as markers of the intermittent chemical activity. The record clearly shows that although a preferred outer scale of dynamics is observed, secondary "tracks" can be observed with fine detail. The oscillations of the front are best observed in the velocity history of the wave recorded along a single line, here taken on the bottom wall of the channel. The velocity record is shown in Figure 5. The detonation wave velocity fluctuates from approximately $1.6V_{CJ}$ to approximately $0.75V_{CJ}$, where V_{CJ} is the ideal Chapman-Jouguet detonation wave velocity. As can be seen, although a distinctive low frequency is observed, due to the formation of a dominant single mode in the narrow computational domain, there exists a large number of instabilities. We have evaluated a power spectrum of this record, and we were not able to isolate any preferred frequency of oscillation of sub-λ oscillations, although the spectrum is quite noisy due to the short amount of data available.

Figure 6 shows the detonation flow field obtained at a single time. The fields of temperature, fluid speed, pressure gradient, density gradient, reaction rate and reactant concentration are shown at the instant where the main frontal triple point is propagating downward. The main feature of these unstable detonations are the unburned pockets convected downstream of the leading front and the resulting weakly turbulent flow field. The pockets originate from the gases shocked by the weaker incident shock, which have much longer ignition delay times than the gases shocked by the Mach stem. Due to the supplementary effect of expansion waves, this gas shocked by the weaker frontal shocks has an induction delay time approximately 100 times greater than the cellular cycle time scale. These pockets react at the smallest scale of resolution by numerical diffusion flames, similar to the effect of real diffusion in the experiments, where it was found that the pockets are consumed by diffusive transport on their boundaries (Radulescu et al., 2005).

Although the turbulent intensity is not as high as in the experiments due to limitations in the numerical resolution, these simulations can nevertheless be used to address qualitatively the global structure of the front and the location of the sonic surface that results from its turbulent large scale structure. The average structure of the reaction zone was obtained by Favre-averaging the flow variables both in time and across the y-direction (Favre, 1965). Favre-averaging denotes taking an average weighted by the local density, to account for the changes in density (and momentum and energy density) at different times and positions in space. Favre-averaging in the frame of reference of the average detonation motion represents seeking the average properties of many statistically similar Lagrangian fluid elements traversing the detonation wave structure.

The time averaging was hence performed in the frame of reference moving with the average detonation wave velocity. The average detonation velocity was difficult to obtain accurately directly from the peak pressure data used to generate Figure 5, since the shock capturing computation does not provide the real peak, but only an approximation. Instead, it was found that a more accurate estimate can be obtained by simply taking time-of-arrival differences

over fixed length intervals, which is mathematically equivalent to taking a time-average of the instantaneous shock velocity field, consistent with our averaging procedure. Discrete times and locations were determined at the locations the main triple point collides with the bottom wall (the peaks in Fig. 5). The peak-to-peak time averages are shown in Figure 7. As can be seen, fluctations remain for the various cell cycles. Even when we averaged over the last parts of the profile ($500 < x < 1000$) corresponding more to a self-sustained propagation, the wave velocity could not be estimated with an uncertainty better than ~1%. The estimated velocity agreed with the ideal CJ velocity within the 1% error.

Because we cannot obtain the average detonation velocity with greater precision than 1%, the spatial and temporal averaging were conducted in the frame of reference moving with the CJ velocity. The averaging procedure in the y-direction and in time was performed in the interval over which the shock propagates from x = 834 to x = 999, i.e., over 6 cell cycles. The solution was outputted 87 times on the given interval and interpolated on a regular grid moving at the CJ velocity. If x' denotes the coordinate in the frame of reference moving with average detonation velocity, W is the width of the window for y-averaging and τ is the total time step in averaging, the pressure and density are averaged in the usual way in time and space:

$$\overline{p}(x') = \frac{1}{\tau}\int_{t_o}^{t_o+\tau}\frac{1}{W}\int_0^w p(x',y,t)\,dydt \qquad 4.1$$

$$\overline{\rho}(x') = \frac{1}{\tau}\int_{t_o}^{t_o+\tau}\frac{1}{W}\int_0^w \rho(x',y,t)\,dydt \qquad 4.2$$

The velocity and reaction progress variable α are Favre-averaged by using the result of (4.2)

$$\widetilde{u}(x') = \frac{1}{\tau}\int_{t_o}^{t_o+\tau}\frac{1}{W}\int_0^w \frac{\rho(x',y,t)u(x',y,t)}{\overline{\rho}(x')}\,dydt \qquad 4.3$$

$$\widetilde{\alpha}(x') = \frac{1}{\tau}\int_{t_o}^{t_o+\tau}\frac{1}{W}\int_0^w \frac{\rho(x',y,t)\alpha(x',y,t)}{\overline{\rho}(x')}\,dydt \qquad 4.4$$

In the averaging procedure, the time elapsed between successive stored models was applied to weigh each model in the time-average process. We used the entire domain width for y-averaging ($W = 6$).

The average pressure, density, reactant concentration α ($\alpha = 1$ is un-reacted gas, $\alpha = 0$ is totally reacted gas) and Mach number are shown in Figure 8, along with the ideal profiles of the steady ZND structure. The Hugoniot diagram representing the path taken by a mean Lagrangian particle in P-v space is shown in Figure 9. Due to the turbulent nature of the front, the state of the particle differs considerably from the ideal Rayleigh line, dictated by one-dimensional conservation of momentum. Clearly, this pre-supposes a large mechanical fluctuation component in the mean momentum conservation. Due to the highly unsteady character of the leading shock structure of the wave, the global rate of chemical reactions is also significantly lower than in the ideal wave, and the reactants are depleted after only approximately 30 $\Delta_{1/2}$. At the rear of the reaction zone, it is also interesting to note that the pressure and density approach the ideal CJ values given by total equilibrium at a distance of approximately $50\Delta_{1/2}$.

Interestingly, this length scale also corresponds to the point where an average sonic surface is developed and the flow Mach number in the detonation frame of reference is unity.

5. Comparison with experiment for high activation energy detonations

It is very interesting to note that the location of the sonic surface determined in the numerical experiments corresponds to approximately 4λ , commensurate with Edwards' (1976) and Soloukhin's (1966) experimental observations. Whether this agreement is fortuitous is not perfectly clear, in view of the shortcomings of the present model (two-dimensionality, poor approximation of dissipative processes). Nevertheless, it is interesting to note that the location of the sonic surface is farther than the chemical relaxation length scale. This pre-supposes that the equilibration of the gasdynamical large pressure and velocity fluctuations may contribute to the delayed establishment of a sonic surface, consistent with Edwards' interpretation of his experimental findings (Edwards et al., 1976). Unfortunately, the limited amount of data could not permit to accurately determine the magnitude of the fluctuating components. This would require very long time-averages in order to obtain statistically converged solutions for the higher order fluctuating quantities. The qualitative magnitude of the pulsations is nevertheless shown in Figure 10, where the pressure realizations across the entire computational domain at a single time are shown only as a function of distance x (corresponding to the same frame shown in Figure 6). The decay of the large amplitude pressure fluctuations seem to correlate roughly with the location of the sonic surface.

It is also instructive to compare the decay of pressure fluctuations with real profiles obtained experimentally. We measured the pressure behind methane-oxygen detonations and simultaneously photographed their structure for an appropriate interpretation of the pressure signal. The experimental set-up consisted of a 25 mm by 100 mm cross-section channel. The detonations were initiated approximately 1000 mm before the test section via an exploding wire delivering on the order of 100 J. In the test section, schlieren photographs were taken and the velocity of the wave was estimated with a pair of PCB pressure transducers spaced 200 mm and mounted flush with the channel wall in Delring housings. The pressure gages have natural frequencies of 500 kHz and are approximately 4 mm in diameter. The calibration provided by the manufacturer (5 mV/PSI) was used in converting the measured voltage into pressure. The gages were covered by a ~1 mm layer of silicone to prevent heating and limit the artificial pressure drop. The pressure signals were averaged in post-processing to eliminate frequencies above 100 kHz. The experiments were performed in stoichiometric methane-oxygen mixtures, at 10 kPa initial pressure. The mixture was chosen such that the cell width (approximately 50 mm (Laberge, 1993)) is sufficiently small such that the reaction zone is not influenced too adversely by wall effects and sufficiently large to permit the resolution of the various features by visualization and pressure measurements. A total of 18 experiments were conducted, from which we determined a wave velocity 3.0 % below the ideal CJ velocity of 2.290 mm/μs with a standard deviation of 2.4% away from the mean. Although wall losses may entirely account for this small velocity deficit, this result suggests nevertheless that waves close to the true self-sustained fully-developed detonations were established.

Figure 11 shows six schlieren photographs and Figure 12 shows the pressure signals measured at the location indicated by an arrow in the photographs. For reference, all photographs were taken with a vertical knife edge, as to capture the density gradients perpendicular to the front, such transverse shocks and reaction layers, with the exception of the third photograph, taken with a horizontal knife edge. Note that manufacturing non-

homogeneities in the glass appear in the horizontal knife edge photograph, and are not present in the other photographs. For reference, time zero in the pressure profiles of Figure 12 corresponds to the time at which the corresponding photograph was taken.

The first conclusion readily obtained from the photographs is that the un-reacted gases observed at lower pressures low mode number detonations (Figure 1) maintain their properties in these higher mode detonations, as clearly indicated by the non-reacted structures observed in the wake of the wave, which appear very spotty. The dark field schlieren photographs also permit to capture the long lived transverse shock waves. Their direction of propagation can be determined by the density gradient sign: dark waves are compression waves going up, light waves are compression waves going down. These can also be individually tracked on the pressure measurements and on the photographs. For example, photograph b was taken 10 μsec after a strong transverse shock reflected from the upper wall. This pressure wave can be seen unambiguously both in the pressure signal and in the photograph. Some 40 μsec later, a strong compression wave, clearly seen in the photograph as a white band, raises the pressure by approximately 1.5 bar. The details of the transverse shock dynamics were found to be quite irreproducible from the different experiments. For example, photograph d) shows a more randomized front structure while the pressure record also indicates higher frequency waves with smaller amplitudes.

The photographs also reveal that these transverse shocks extend deep in the reacted gases, for distances much longer than the apparent spotty regions of fluctuating high density gradients associated with chemical reactions at the front. The measured pressure fluctuations also decay slowly, and their decay correlates very well with the apparent strength of transverse density discontinuities associated with these strong transverse shocks observed on the photographs. The pressure pulsations are approximately 10 to 40 % of the peak pressures over the first pulsation, and decay to much smaller amplitudes behind the front.

A mean pressure profile was obtained by averaging 11 pressure traces such those presented in Figure 12. The resulting average profile is shown in Figure 13. The pressure is found to decay to the ideal CJ pressure of 2.7 bar approximately 120 μsec after the wave passage. Since the wave propagates at an average velocity of approximately 2.22 mm/μsec, this means that the pressure decays to a value close to the ideal CJ value at approximately ~270 mm behind the front or approximately 5 cell widths λ. This is in good agreement with the results of Edwards and Vasil'ev. In contrast, the thickness of the "spotty" region at the front obtained from the schlieren photographs, corresponding to the large density gradients of the un-reacted pockets interfaces, is less than 20 mm, or less than half a cell width.

The delayed pressure decay in Figure 13 can difficultly be explained by slow reactions in the product gases slowly liberating their chemical energy. We performed a calculation of the ZND pressure profile using the Lutz et al. (1988) mechanism for methane oxidation and a code developed by Shepherd (1986). The pressure profile obtained is shown in Figure 12. Clearly, the structure approaches a square-wave profile, where practically all the energy is liberated after a thermally neutral induction zone of approximately 5 mm and the pressure falls to nearly its equilibrium value thereafter. The two possibilities that can account for the large discrepancy in decay rates of computed and experimental pressure are that either unsteady fluctuations have a profound effect on re-combination kinetics, delaying the energy release, or that the delayed pressure decay in the experiments is due to the afore-mentioned mechanism of turbulence via dissipation of energy. Although the first scenario cannot be ruled out, the latter scenario appears to be favored by the present numerical experiments, which also suggest that the appearance of a

sonic surface is more closely related to the relaxation of mechanical and thermal fluctuations, rather than the termination of the chemical reactions, consistent with Edwards' interpretations (Edwards et al, 1978). This finding remains to be confirmed in future studies, where a better resolution in both numerical and experimental measurements are needed.

6. Numerical results for low activation energy detonations

The numerical results obtained from the highly unstable detonations are limited due to the lack of resolution in capturing the correct dissipation rates and decay of fluctuations, and the limited time spans used to obtain the statistical properties. For this reason, we pursued our investigation of the hydrodynamic structure of detonations with detonations characterized by significantly lower instabilities, which can be solved for a smaller computational price and more accurate statistical properties can be obtained. For such mixtures, previous computations show that all pertinent structures can reliably be captured with reasonable resolution levels (Sharpe, 2001).

Exactly the same averaging procedures as described above were also applied to these weakly unstable detonations obtained by taking $E_a/RT_o = 27$, $Q/RT_o = 50$ and $\gamma = 1.2$. Figure 14 shows the detonation velocity profile recorded on the bottom wall of the domain. Figure 15 shows the cell-averaged velocity profile. Because of the good reproducibility of the detonation features and quasi-periodicity of the structure, the average detonation velocity was estimated with greater accuracy. After the initiation transient during which the wave is decaying, the average velocity was found to be 0.5% lower than CJ, with a confidence level of ~0.3%.

Typical snapshots of the reaction zone profiles are shown in Figure 16 for temperature, pressure gradient and degree of reaction. Clearly, due to the much lower activation energy with respect to the case investigated above, most of the reactions now occur in the close vicinity of the front, and the structure is a lot less complex than for the detonations shown in Figures 5 and 10. The structure resembles more closely that of argon-diluted mixtures with low-activation energies (Pintgen et al., 2003).

The average reaction zone structure was determined in the interval $364 < x / \Delta_{1/2} < 707$. A total of 955 saved models at successive time intervals were used to generate the time-averaged solution. The Favre-averaged reaction zone profiles for pressure, density, reaction progress variable α and Mach number are shown in Figure 17. The path taken by an average fluid element is shown in Figure 18. The departure of the reaction zone profiles from the ideal ZND structure is a less noticeable, although the peak of the profiles differs substantially due to the spatial and temporal averaging over the pulsating leading front. A sonic plane is developed at approximately $12\Delta_{1/2}$ behind the front, much shorter than for the really unstable detonations considered above. Beyond the sonic point, the unsteady Taylor expansion exhibits fluctuations, possibly vestigial transients of the initiation process or weaker secondary shocks traveling very close to sonic velocity in the vicinity of the sonic surface. At the sonic plane, the mean pressure is found lower than the CJ value by approximately 1%.

Since the velocity of the wave is found lower than the ideal CJ value, it is interesting to measure the partition of the various energy modes in the detonation structure. By inspection, following an average fluid particle traversing this statistically steady detonation structure, the total energy of a fluid particle is conserved and partitioned between mean enthalpy, mean kinetic, chemical potential energy and turbulent energy, according to:

$$E_{tot} = \frac{\gamma}{\gamma - 1}\frac{\overline{p}}{\overline{\rho}} + \frac{1}{2}\widetilde{u}^2 + \alpha Q + E_{turb} \qquad 6.1$$

Figure 19 shows the magnitude of the various terms. The turbulent energy was evaluated by subtracting the mean energies from the total energy available in the undisturbed gas. After the shock transition, where the turbulent energy peaks, it slowly decays to less than 1% of the total energy. It is interesting to note that at the sonic point, there is still energy in the form of potential chemical energy (~0.3% of E_{tot}) and turbulent energy (~0.5% of E_{tot}). This total energy of ~1% is hence liberated past the sonic point, and does not influence the detonation wave. Since the detonation velocity varies with the square root of the available energy, an energy deficit δQ is related to a velocity deficit δD by

$$\frac{\delta D}{D} = \frac{1}{2}\frac{dQ}{Q} \qquad 6.2$$

The energy deficit of ~1% is thus in perfect agreement with the observed velocity deficit of ~0.5%.

7. Further discussions

The conclusion from the above numerical experiments is that substantial differences are found between the idealized model and the average structure of detonations. In general, it was found that cellular detonations are well characterized by an average sonic surface, located at a finite distance from the front and separating the statistically steady detonation structure from the unsteady expansions. For the more regular detonations where more accurate results could be obtained, it was found that not all the available energy is released at the sonic surface and the detonation can suffer from a velocity deficit. Large quantitative differences were found between highly unstable detonations with an intense turbulent reaction zone structure and the weakly-unstable detonations. For the highly unstable detonation, the hydrodynamic thickness is significantly longer than the ideal wave, consistent with experimental observation. It appears that this long length scale is due to the delay of chemical and thermal relaxation due to the formation of un-reacted pockets, which also contributes to increase the level of mechanical fluctuations in the flowfield (pressure fluctuations). The location of the sonic surface in this case seems to correlate best with the gas-dynamical relaxation of these mechanical fluctuations. The same processes also operate in the weakly unstable detonations. However, the amplitude of the fluctuations is lower and the gases are burned much more rapidly. As a result, the structure of weakly unstable detonations is only approximately half a cell width, and resembles much more closely the ideal ZND profile. In both cases, the hydrodynamic thickness of the wave captures correctly the processes of chemical, mechanical and thermal relaxation towards equilibrium.

For the irregular structure detonations, since a well-defined motion of the wave in a single dimension can be defined (normal to the wave), on a length scale sufficiently larger than the sub-cell fluctuations (such that "mean" normal can be defined), and that the thickness of the wave is also sufficiently long to permit averaging over the small scale oscillations, it appears that a one-dimensional unsteady stochastic model can be formulated, in the direction of propagation of the wave. Formally, we Favre-filter the governing Navier-Stokes equations in the frame of reference of the wave by the same procedure described above. We use the hypothesis that a mean constant detonation velocity can be defined, which is well verified empirically from both numerical simulation and experiments.

In the frame of reference of the mean detonation wave propagation, the resulting Favre-averaged governing equations (neglecting the molecular transport terms) become

$$\frac{d}{dx}(\rho u) = 0 \tag{7.1}$$

$$\frac{d}{dx}\left(\rho u^2 + p\right) = -\frac{d}{dx}\overline{\rho u'^2} \tag{7.2}$$

$$\frac{d}{dx}\left(\rho u\left(\frac{\gamma}{\gamma-1}\frac{p}{\rho} + \frac{1}{2}u^2 + \frac{\lambda q}{\gamma M_{CJ}^2}\right)\right) = -\frac{d}{dx}\left(\frac{j+2}{2}u\overline{\rho u'^2} + \frac{j}{2}\overline{\rho u'^3} + \frac{1}{\gamma M_{CJ}^2}\overline{\rho u'\lambda' q} + \overline{\rho u' h'}\right) \equiv g \tag{7.3}$$

where j denotes the dimensionality of the problem ($j = 2$ for two dimensions and $j = 3$ for three-dimensions). The left hand sides represent the conservation of mass, momentum and energy of an average fluid element traversing the detonation wave structure. The right hand sides are the filtered terms which now only depend on a single axial distance x by virtue of the averaging procedure. These source terms need to be modeled in terms of the other dependent and independent variables and are only a consequence of the turbulence levels inside the detonation wave itself. Similar decompositions into mean and fluctuating components were also introduced by a number of authors in the past (Voitsekhovskii et al. 1963, White 1966, Strehlow 1971, Panton 1971, Rybanin 1966, Nikolaev & Zak 1969), although only the fluctuations due to velocity were considered.

One of the implications of the above model on the global structure of the wave and the existence of a sonic surface can be obtained without addressing explicitly the functional form of the source terms, which will be discussed later. Instead, we shall assume that the turbulent source terms can be modeled by supplementary relaxation processes of general form occurring in the detonation structure. The source term in the momentum equation governs the mechanical relaxation. Fluctuations in the energy modes provides for an energy relaxation process, via gasdynamic expansions, energy cascades and molecular dissipation. Taking time t instead of distance x' as the only independent variable, the governing equations can be written as

$$\frac{dx'}{dt} = \widetilde{u} \tag{7.4}$$

$$\frac{d(\overline{\rho}\widetilde{u})}{dt} = 0 \tag{7.5}$$

$$\frac{d\left(\overline{p} + \overline{\rho}\widetilde{u}^2\right)}{dt} = -\overline{\rho}\dot{f} \tag{7.6}$$

$$\frac{d}{dt}\left(\frac{\gamma}{\gamma-1}\frac{\overline{p}}{\overline{\rho}} + \frac{1}{2}\widetilde{u}^2\right) = -\dot{\alpha}Q - \dot{g} \tag{7.7}$$

where the time derivative or the dot represents the Lagrangian time derivative following the average location of an "average" fluid particle in the reaction zone. At mechanical and thermal equilibrium, we have $\dot{f} = \dot{g} = 0$. The reaction rate $\dot{\alpha}$ also appears as a source term in the energy equation, and describes the relaxation to chemical equilibrium $\dot{\alpha} \to 0$. The reaction rate itself needs to be formulated in terms of the other dependent average variables:

$$\dot{\alpha} = \dot{\alpha}(x, p, \rho, u, f, g, \ldots) \tag{7.8}$$

The state at the end of the reaction zone, when the flow is sonic, cannot be obtained based on the Chapman-Jouguet criterion of equilibrium, but has to be determined from the integration of the

governing equations for the structure between the leading shock and sonic surface. Upon re-arrangement of the governing equations, we can obtain expressions for the evolution of all the dependent variables

$$\frac{\dot{u}}{u} = \frac{\Phi}{\eta}\,;\ \frac{\dot{\rho}}{\rho} = -\frac{\Phi}{\eta}\ ;\ \frac{\dot{p}}{\rho u^2} = -\frac{\Phi + M^2 \dot{f}\eta}{\eta} \qquad 7.9$$

where

$$\Phi \equiv -(\gamma-1)\dot{\alpha}Qc^2 + \gamma\dot{f}c^2 - (\gamma-1)\dot{g}c^2 \qquad 7.10$$

$$\eta \equiv 1 - u^2/c^2 = 1 - M^2 \qquad 7.11$$

By inspection, the solution is singular at the sonic surface, where $\eta = 0$. The unique solution for the reaction zone structure is by requiring that simultaneously $\Phi = 0$. This is the usual "*generalized CJ criterion*" (Bdzil 1981), which is generic to the presence of any source terms in the governing equations (friction, heat loss, mass loss in the mass equation, etc…). The generalized CJ criterion is satisfied for only a specific detonation wave velocity, which is the "eigenvalue". Along with this eigenvalue solution and the shock state, the profiles can be integrated and the location for the sonic surface can be determined. Clearly, the location of the sonic surface is dictated by the balance between the different relaxation rates $\dot{\alpha}$, $\dot{f}$ and $\dot{g}$. It is worthwhile checking the results obtained from the numerical simulations above for the weakly unstable case where a statictically converged solutions were obtained. Figure 20 shows both thermicity Φ and sonicity η, obtained numerically from averaging the cellular detonation with $E_a/RT_o = 27$ discussed above. The sonic plane corresponds to the point where the thermicity falls to zero. Whether the rear of the detonation structure is always dictated by an eigenvalue structure is not perfectly clear at present. The requirement that the thermicity Φ fall to zero before all the energy has been released may not be true in general. For the weakly unstable detonations, an eigenvalue type is however supported by our calculations. It is not clear whether the same holds for the more unstable detonations, characterized by much stronger fluctuations. More accurate calculations and much more accurate statistics than the ones presented here would be required to address this question satisfactorily.

Closure of the model suggested also appears a very difficult task. Current turbulence models for deflagrations (e.g., see Peters 2000) are inadequate due to their failure to address the compressibility effects which are important in the reaction zone of cellular detonations. In low speed turbulence, vortex-vortex interactions is the dominant turbulence mechanism where turbulent kinetic energy cascades to small dissipative scales. When compressibility effects are dominant and strong pressure fluctuations are present, then shock-vortex interactions and shock-shock interactions (which produce additional vorticity via the shear layers generated at triple shock Mach interactions) can be equally important as vorticity producing mechanisms. Furthermore, chemical reactions produce strong density gradient fields and interfaces. Interacting pressure and density gradients produce vorticity by the baroclinic $\nabla\rho \times \nabla p$ vorticity generation mechanism. Shock interactions with density interfaces also lead to turbulence production by the same mechanism, also known as the Richtmyer-Meshkov-Markstein instability in the context of shock-flame interactions. Thus, turbulence models capturing these compressible turbulence mechanisms must be developed to serve as source terms in the one-dimensional formulation. The turbulent reaction model must also reflect the compressible turbulence mechanisms. Current models for the description of turbulent deflagrations (e.g., laminar flamelet models) are inadequate for cellular detonations. Furthermore, in detonations,

the turbulent fluctuations (pressure, velocity and density) are a direct consequence of the exothermicity, whereas in deflagration studies, it is assumed to originate externally (e.g., turbulent pipe flow). The development of these source terms would thus be a challenging task.

However, within a purely empirical framework, a relaxation formalism can still be sought to characterize the cellular structure of detonations by simply specifying empirical relaxation rate laws for the chemical, mechanical and energetic relaxation processes towards equilibrium. The various (postulated) relaxation rate terms in the assumed equations can be easily calibrated against real or numerical experiments for the structure. When properly calibrated, this can give the desired predictive model for the detonation structure and dynamic parameters.

8. Conclusions

The present work considered whether cellular detonations can be approximated in a one-dimensional stochastic framework. The numerical and real experiments suggest that a well defined thickness of the reaction zone structure can be taken as the distance from the front to the sonic surface, separating the statistically steady reaction zone structure from the trailing expansion waves. Since this length scale is larger than all length scales associated with the dynamics of a detonation wave, an attempt to model the fluctuating phenomena in a hydrodynamic average sense is valid. The properties of both highly unstable and weakly unstable detonations were addressed by Favre-averaging the profiles obtained. It was found that the relaxation of mechanical and thermal fluctuations affected in a non-trivial way the location of the sonic surface. A relaxation formalism was postulated to account for the effect of fluctuations on the location of the sonic surface. Although these terms can be calibrated from experiment, closure for the fluctuating terms appears a formidable task in view of the complexities of real detonations involving compressible exothermic turbulence.

Acknowledgements

We wish to acknowledge the financial support of FCAR, NSERC, EPSRC, DSTL, and the BP Carbon Mitigation Initiative at Princeton University for supporting this research.

References

Austin J. The Role of Instability in Gaseous Detonation. Ph.D. thesis, California Institute of Technology, Pasadena, California, June 2003.

Austin J. M., Pintgen F. & Shepherd J. E. 2005 Reaction zones in highly unstable detonations. *Proc. Combust. Inst.* 30, 1849-1857.

Bdzil J. B. 1981 Steady state two dimensional detonation. *J. Fluid Mech.* 108, 195 – 226.

Edwards D. H., Jones A. J. & Phillips D. E. 1976 Location of Chapman - Jouguet surface in a multiheaded detonation-wave. *J. Phys. D: Applied Physics.* 9, 1331-1342.

Favre A. 1965 Equations des gas turbulents compressibles. *Journal de Mécanique* 4, 361-421.

Fickett, W., & Davis, W. C., *Detonation*. University of California Press, 1979.

Gavrikov A. I., Efimenko A. A. & Dorofeev S. B. 2000 A model for detonation cell size prediction from chemical kinetics. *Combust. and Flame*. 120(1-2), 19-33.

Henrick A. K., Aslam A.D. & Powers J. M. Highly accurate numerical simulations of pulsating one-dimensional detonation. 43rd AIAA Aerospace Sciences Meeting and Exhibit, 10-13 January 2005, Reno, Nevada, paper AIAA 2005-1131.

Kasimov A. R. & Stewart D. S. 2004 On the dynamics of self-sustained one-dimensional detonations: a numerical study in the shock-attached frame. *Phys. Fluids*. 16(10), 3566-3578.

Laberge S., Knystautas R. & Lee J. H. S. 1993 Propagation and extinction of detonation waves in tube bundles. *Prog. Astro. Aero*. 153, 381–396.

Landau L.D. & Lifshitz E.M. 2003 *Fluid Mechanics, Second Edition*. Elsevier.

Lee J. H., Soloukhin R. I. & Oppenheim A. K. 1969 Current views on gaseous detonation. *Astronaut. Acta* 14, 565-584.

Lee, J. H. 1984 Dynamic parameters of gaseous detonations. *Annu. Rev. Fluid. Mech.* 16, 311–336.

Lundstrom, E. A. & Oppenheim, A. K. 1969 On the influence of non-steadiness on the thickness of the detonation wave. *Proc. Roy. Soc. A*. 310, 463-478.

Lutz, A. E., Kee, R. J., Miller, J. A., Dwyer, H. A., & Oppenheim, A. K. 1988 Dynamic effects of autoignition centers for hydrogen and C1,2-hydrocarbon fuels. *Proc. Combust. Inst.* 22, 1683-1693.

Ng, H. D., Higgins, A. J., Kiyanda, C. B., Radulescu, M. I., Lee, J. H. S., Bates, K. R., & Nikiforakis N. 2005 Nonlinear dynamics and chaos analysis of one-dimensional pulsating detonations. *Combust. Theory and Modelling.* 9(1), 159-170.

Nikolaev, Yu. A. & Zak D. V. 1989 Quasi-one-dimensional model of self-sustaining multifront gas detonation with losses and turbulence taken into account. *Combust. Explo. and Shock Waves* 25(2), 103-112.

Panton, R. 1971 Effects of structure on average properties of two-dimensional detonations. *Combust. and Flame* 16, 75-82.

Peters, N. 2000 *Turbulent combustion*. Cambridge.

Pintgen, F., Eckett, C. A., Austin, J. M. & Shepherd J. E. 2003 Direct observations of reaction zone structure in propagating detonations. *Combust. and Flame* 133(3), 211-229.

Radulescu, M.I. & Lee, J.H.S. 2002 The failure mechanism of gaseous detonations: experiments in porous wall tubes. *Combust. and Flame* 131, 29–46.

Radulescu, M. I., Sharpe G. J., Lee J. H. S., Kiyanda C., Higgins A. J. & Hanson R. K. 2005 The ignition mechanism in irregular structure gaseous detonations. *Proc. Combust. Inst*. 30, 1859-1867.

Rybanin, S. S. 1966 Turbulence in detonations. Combust. Explo. and Shock Waves 2(1), 29-35.

Sharpe, G. J. 2001 Transverse waves in numerical simulations of cellular detonations. *J. Fluid Mech.* 447, 31-51.

Shepherd, J. E. 1986 Chemical kinetics of hydrogen-air-diluent mixtures. *Prog. Astro. Aero.* 106,263-293.

Soloukhin, R. I. 1966 Multiheaded structure of gaseous detonation. *Combust. and Flame* 10, 51-58.

Soloukhin, R. I.1969 Nonstationary phenomena in gaseous detonation. *Proc. Combust. Inst.* 12, 799-807.

Strehlow, R. A. 1971 Detonation structure and gross properties. *Combust. Sci. and Tech.* 4, 65-71.

Taylor, G. 1950 The dynamics of the combustion products behind plane and spherical detonation fronts in explosives. *Proc. Roy. Soc. A*. 200(1061), 235-247.

Vasil'ev A. A., Gavrilenko T. P. & Topchian M. E. 1972 On the Chapman-Jouguet surface in multi-headed gaseous detonations. *Astronaut. Acta.* 17, 499-502.

Frisch, U. 1995 *Turbulence*. Cambridge

Voitsekhovskii, B.V., Mitrofanov, V. V. & Topchian, M.E. 1963 *Structure of a detonation front in gases*. Izd. Akad. Nauk SSSR, Novosibirsk.

Weber, M. & Olivier, H. 2004 The thickness of detonation waves visualized by slight obstacles. *Shock Waves* 13(5), 351-365.

Williams, F. A. 1985 *Combustion Theory, Second Edition*. Perseus Books Publishing.

White, D. R. 1961 Turbulent structure of gaseous detonation. *Phys. Fluids*. 4, 465-480.

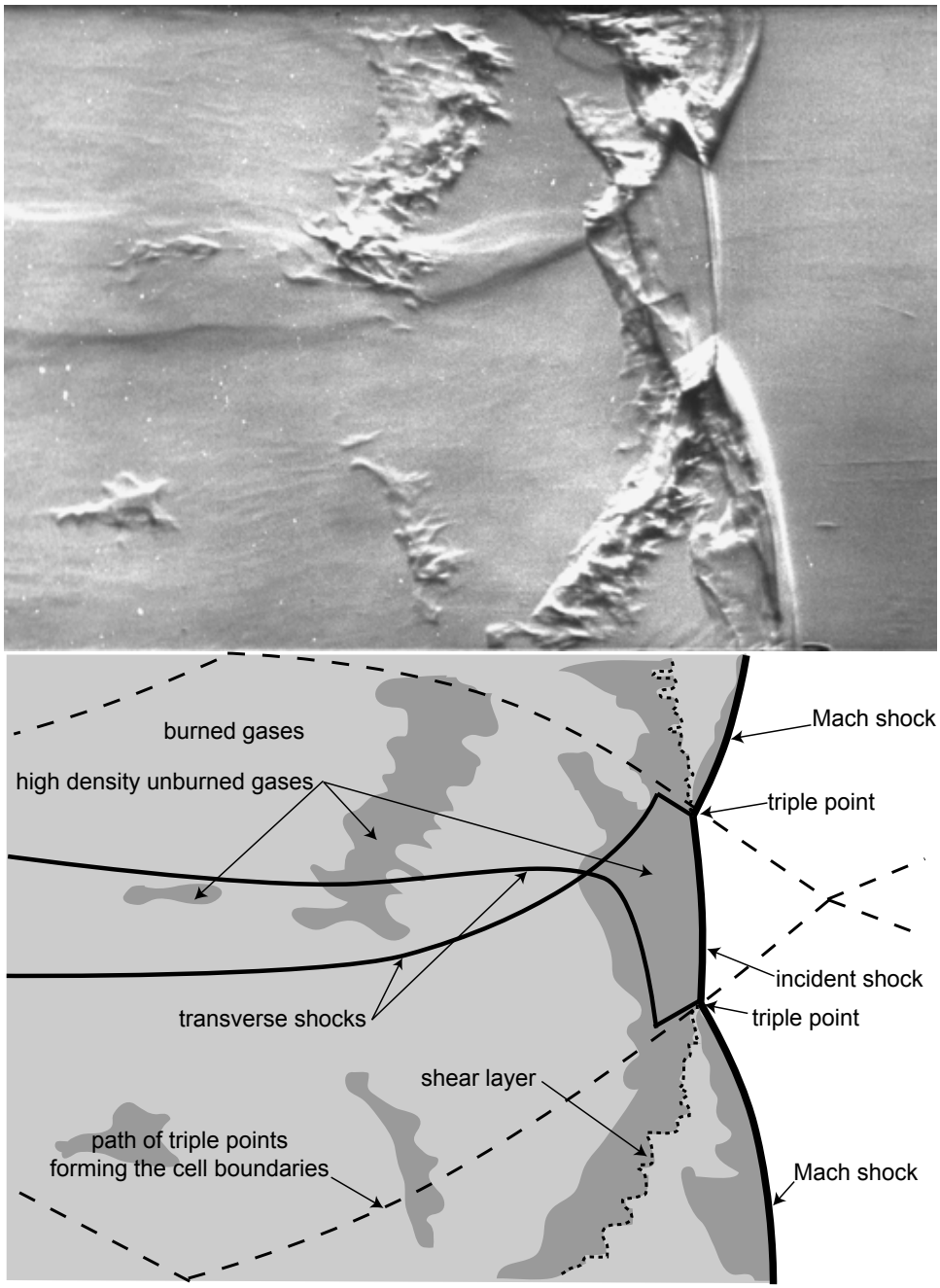

Figure 1 Schlieren photograph of detonation structure in a $CH_4 + 2O_2$ mixture at 3.4 kPa initial pressure in a 25 mm by 100 mm cross-section channel and explanatory sketch

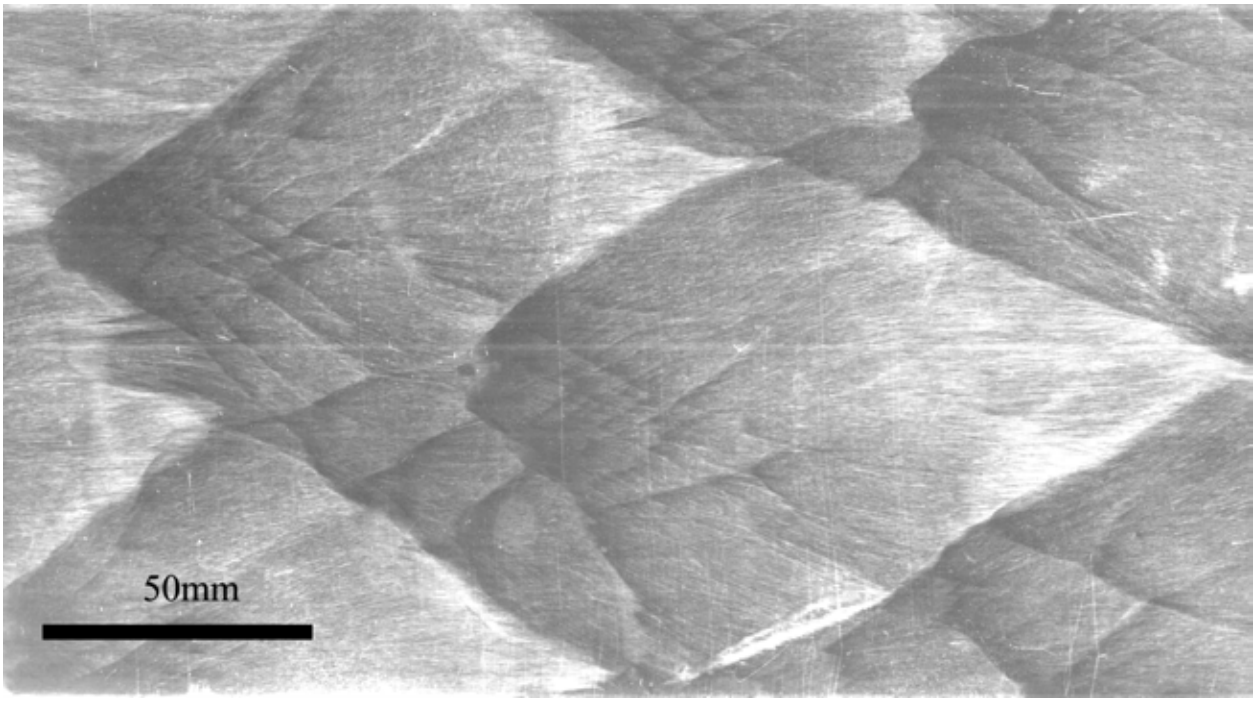

Figure 2 Soot foil from detonation in CH_4-$2O_2$-0.2Air at 11 kPa initial pressure obtained in a 18 mm by 127 mm channel; detonation propagated from left to right.

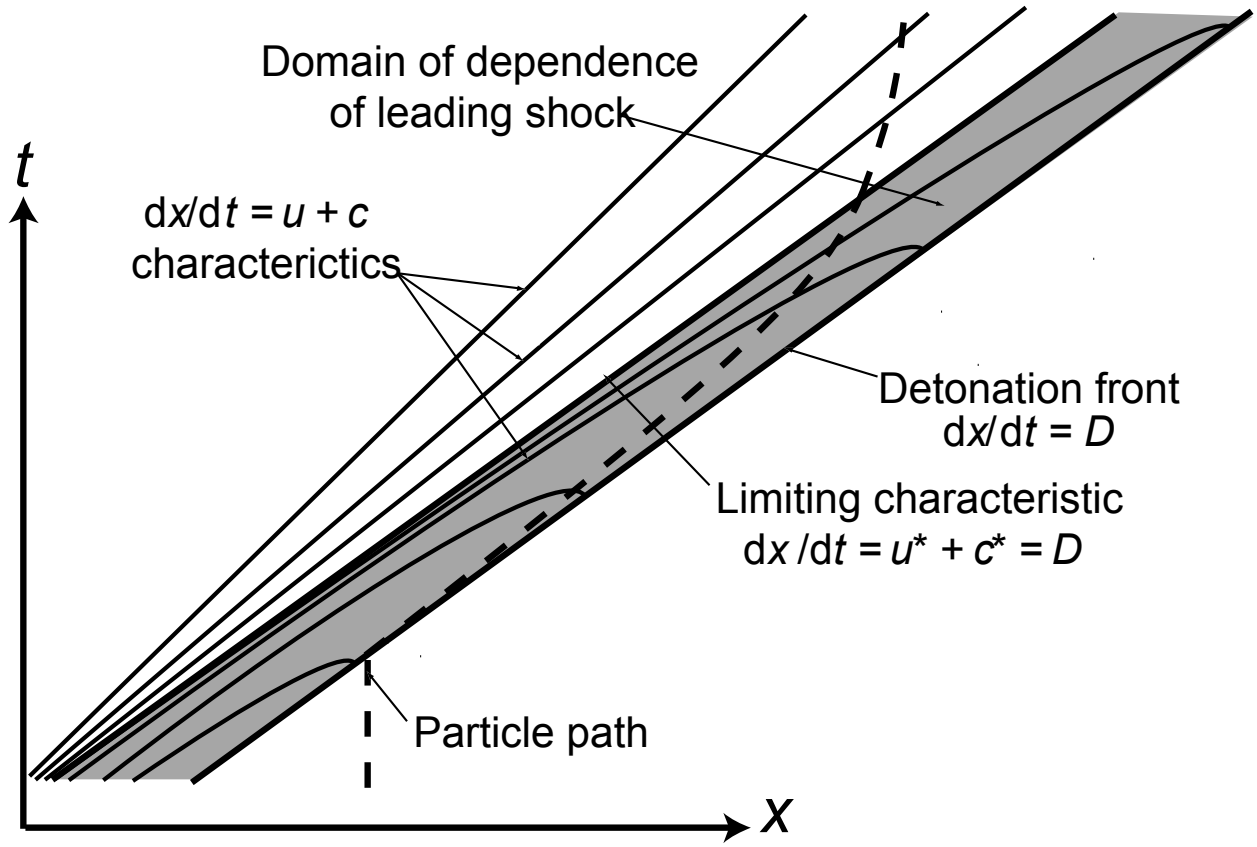

Figure 3 x-t diagram illustrating the limiting characteristic at the sonic locus in the detonation frame of reference

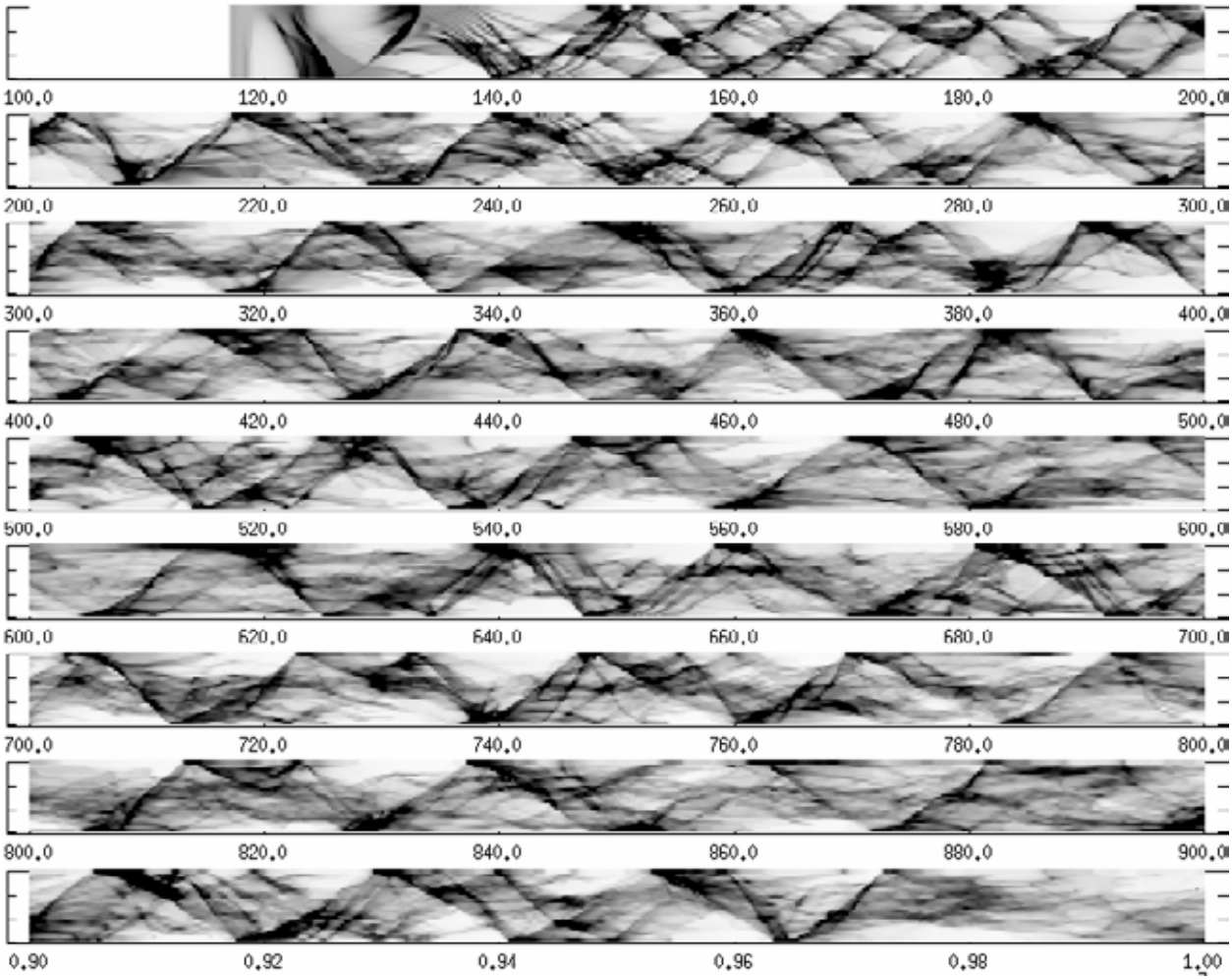

Figure 4 Time-integrated exothermicity illustrating the cellular structure for the $E_a/RT_o = 63.7$ detonation

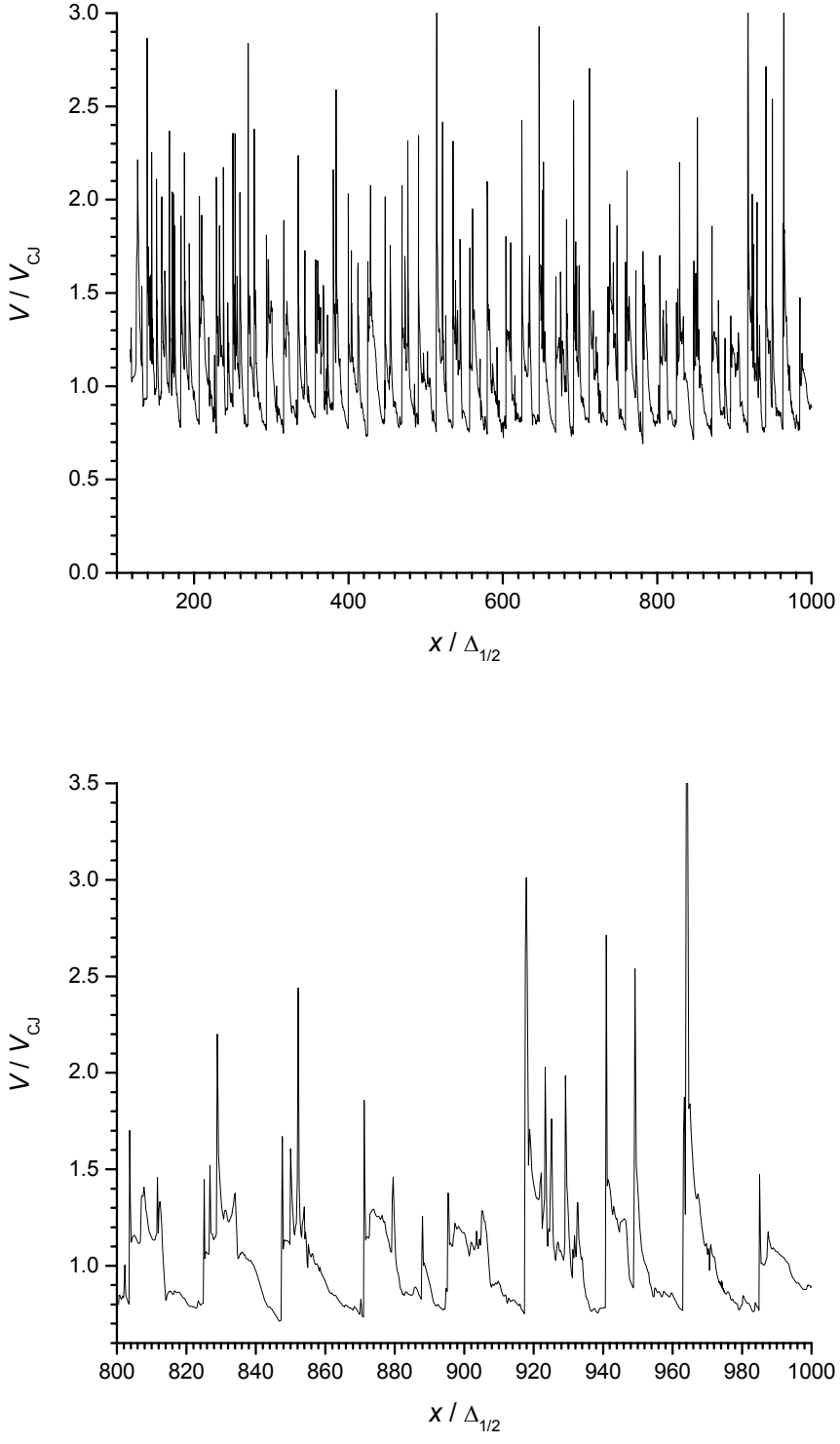

Figure 5 Velocity of the leading front recorded along the bottom wall of the computational domain; a) for the entire domain, b) detail

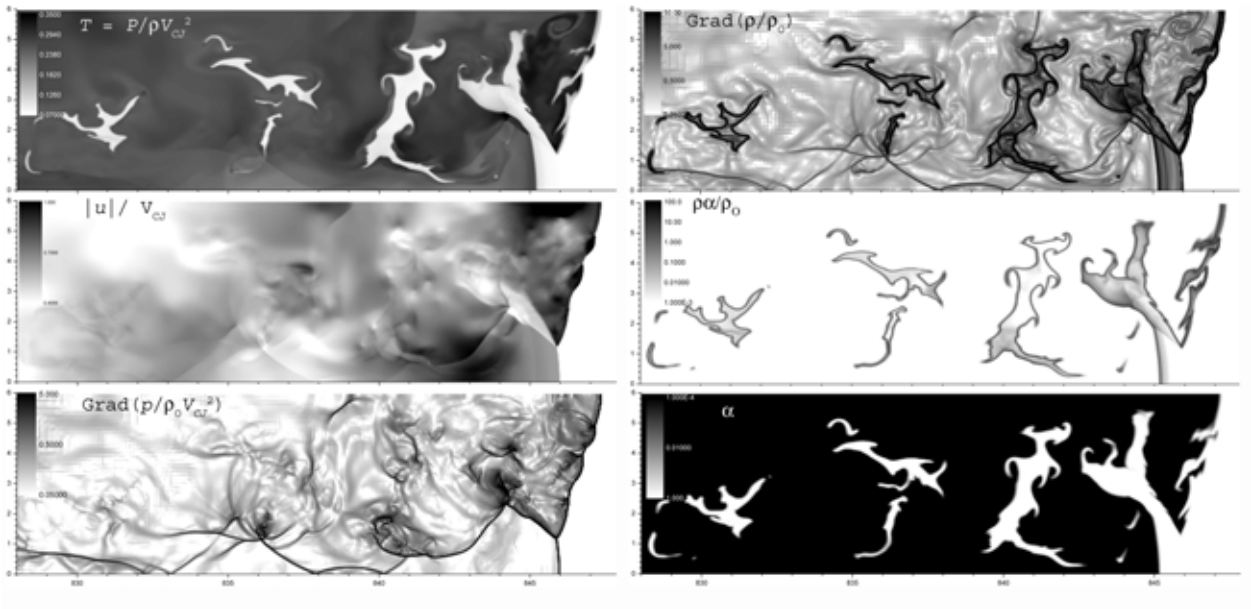

Figure 6 Instantaneous temperature, particle velocity, pressure gradient, density gradient, reaction rate and reactant concentration for an unstable detonation wave ($E_a/RT_o = 63.7$)

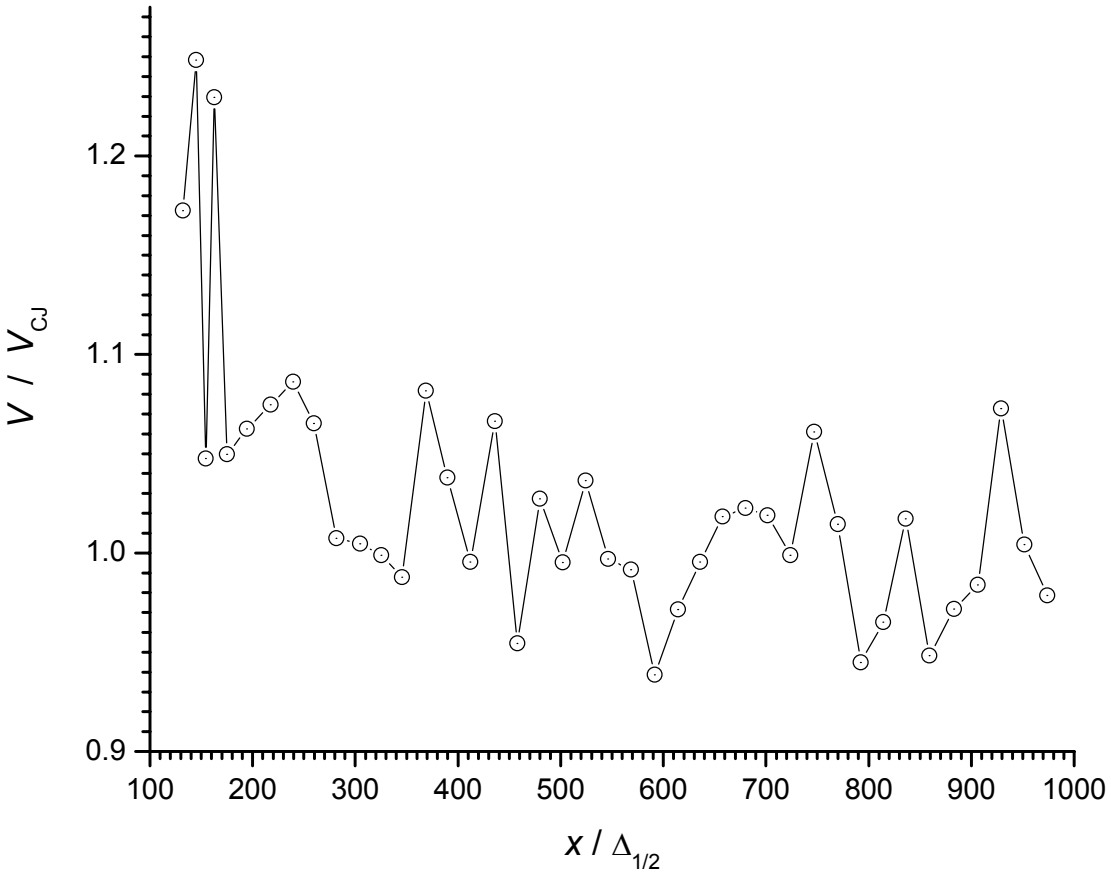

Figure 7 Cell-averaged velocity history of profile of Figure 5

Figure 8

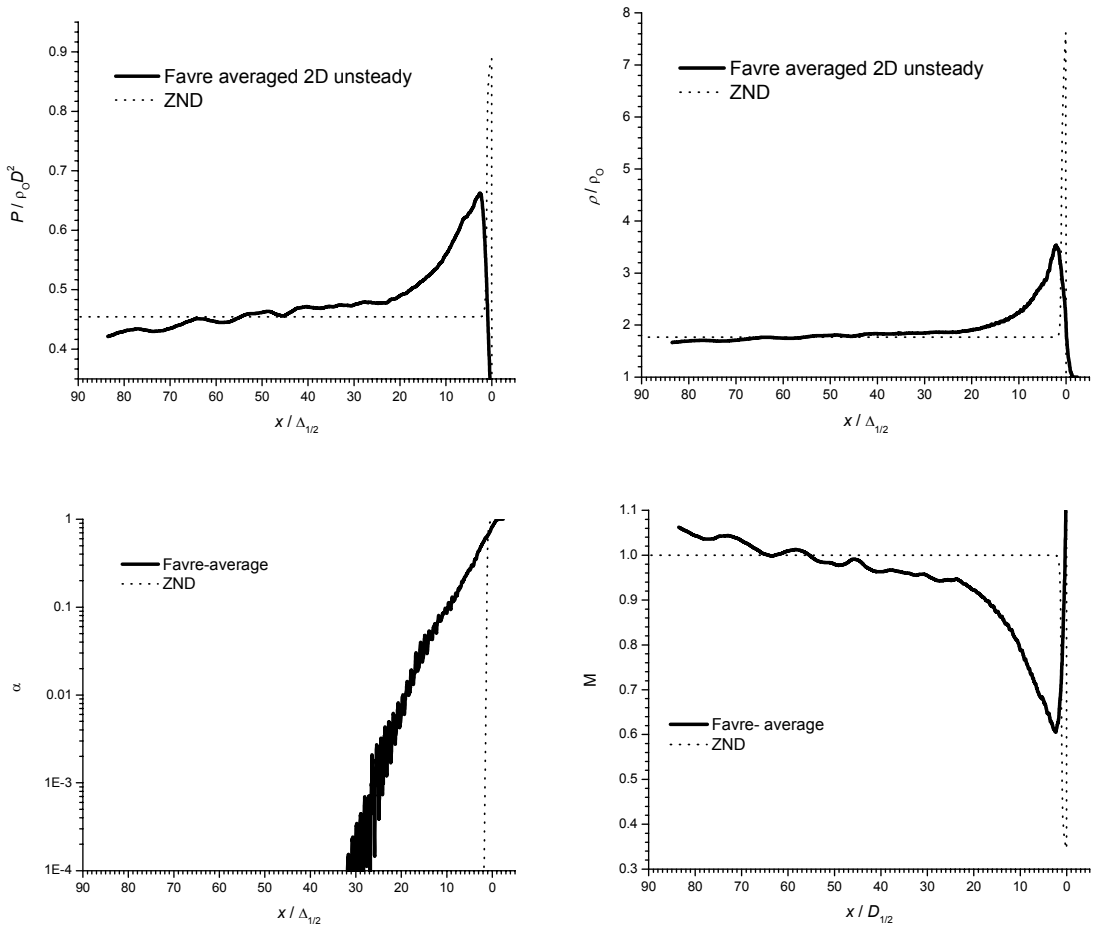

Figure 8 Favre-averaged pressure, density, reactant concentration and Mach number profiles for the highly unstable detonation wave; the ZND profiles are shown for comparison

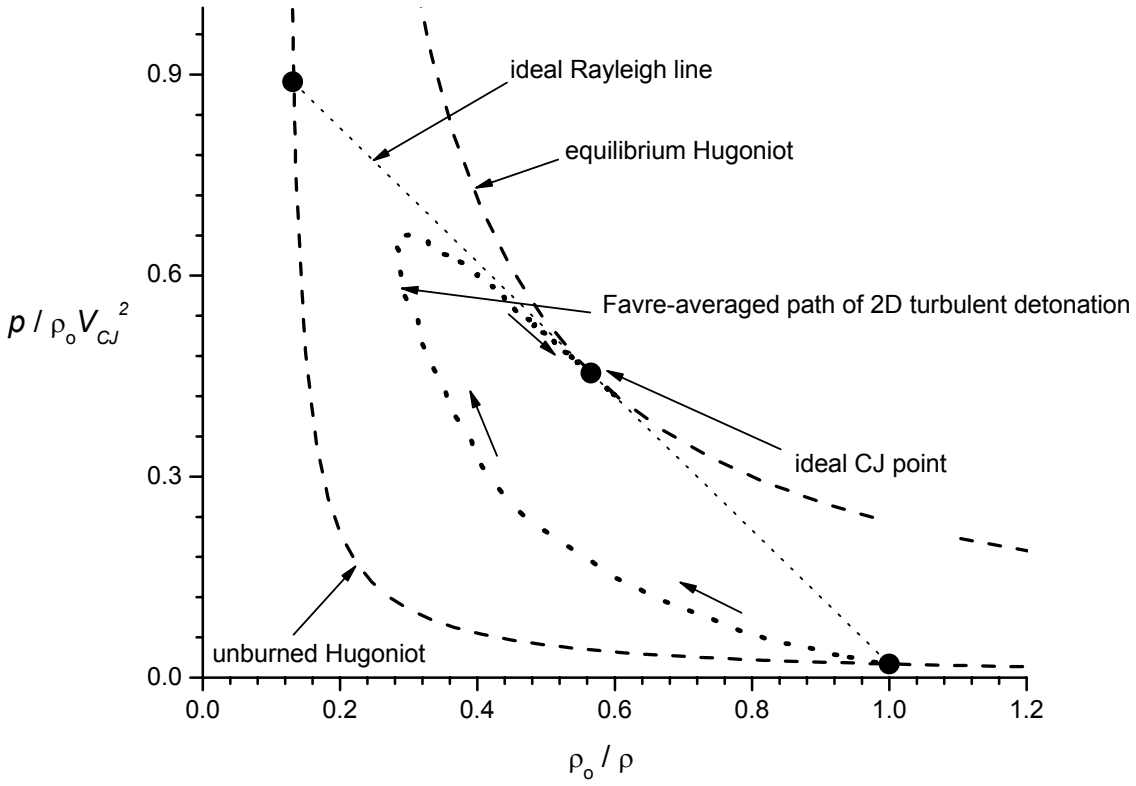

Figure 9 The integral curve of a mean Lagrangian particle traversing the detonation wave structure on a *P*-*v* diagram

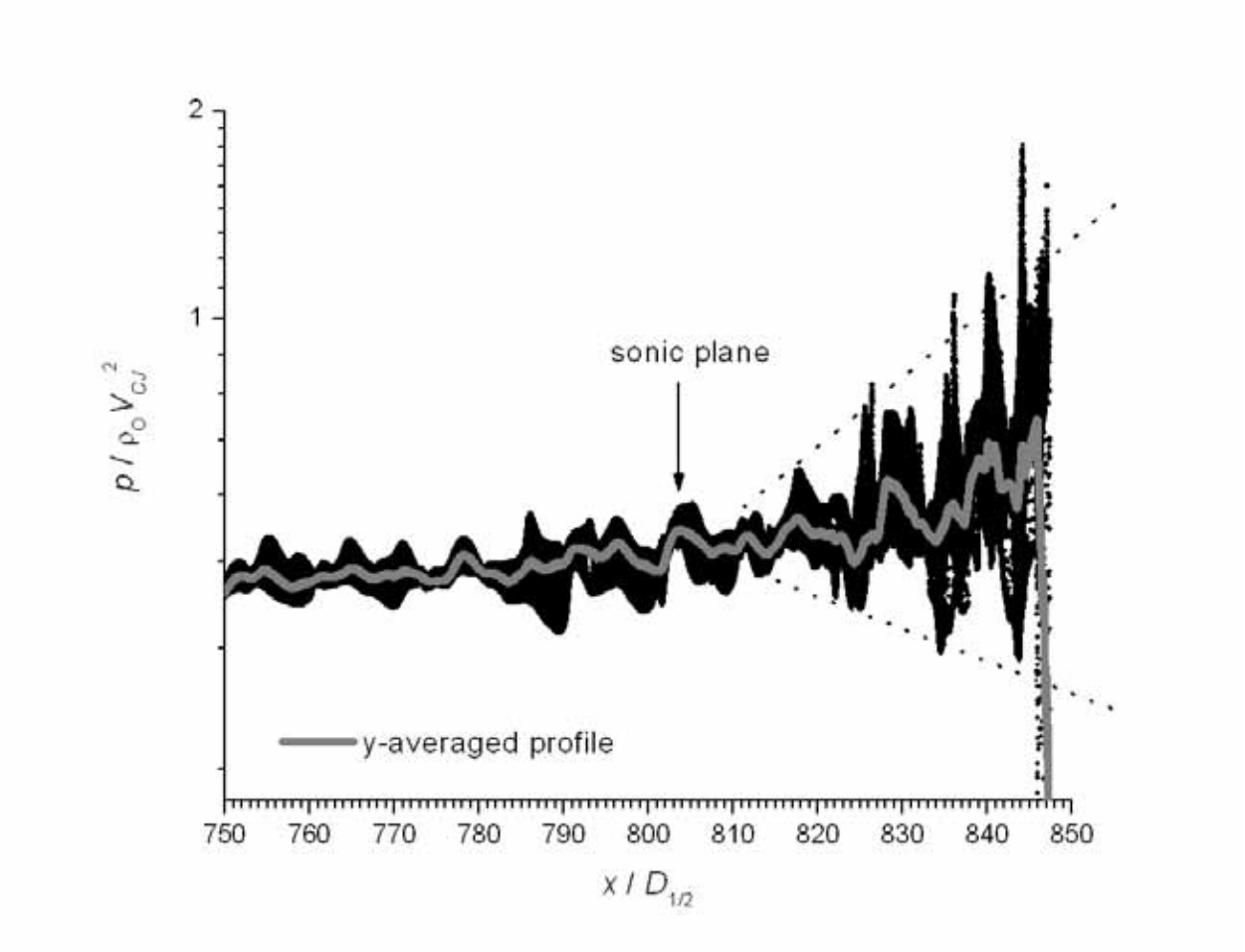

Figure 10 The magnitude of pressure fluctuations for the detonation illustrated in Figure 6

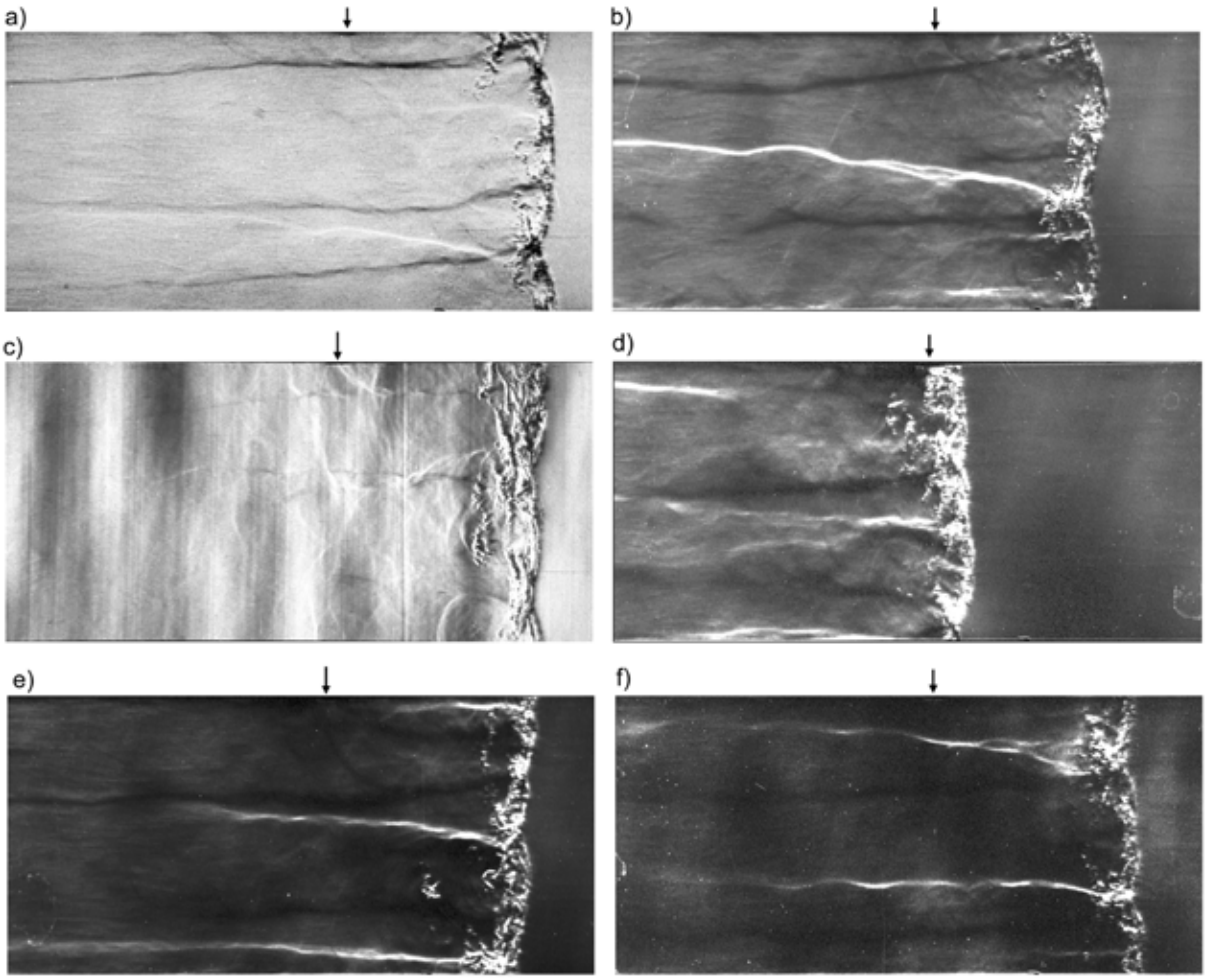

Figure 11 Schlieren photographs of the detonation structure in $CH_4 + 2O_2$ mixtures at 10 kPa initial pressure in a 100 mm by 25 mm cross-section channel, the arrow indicates the location of the pressure transducer

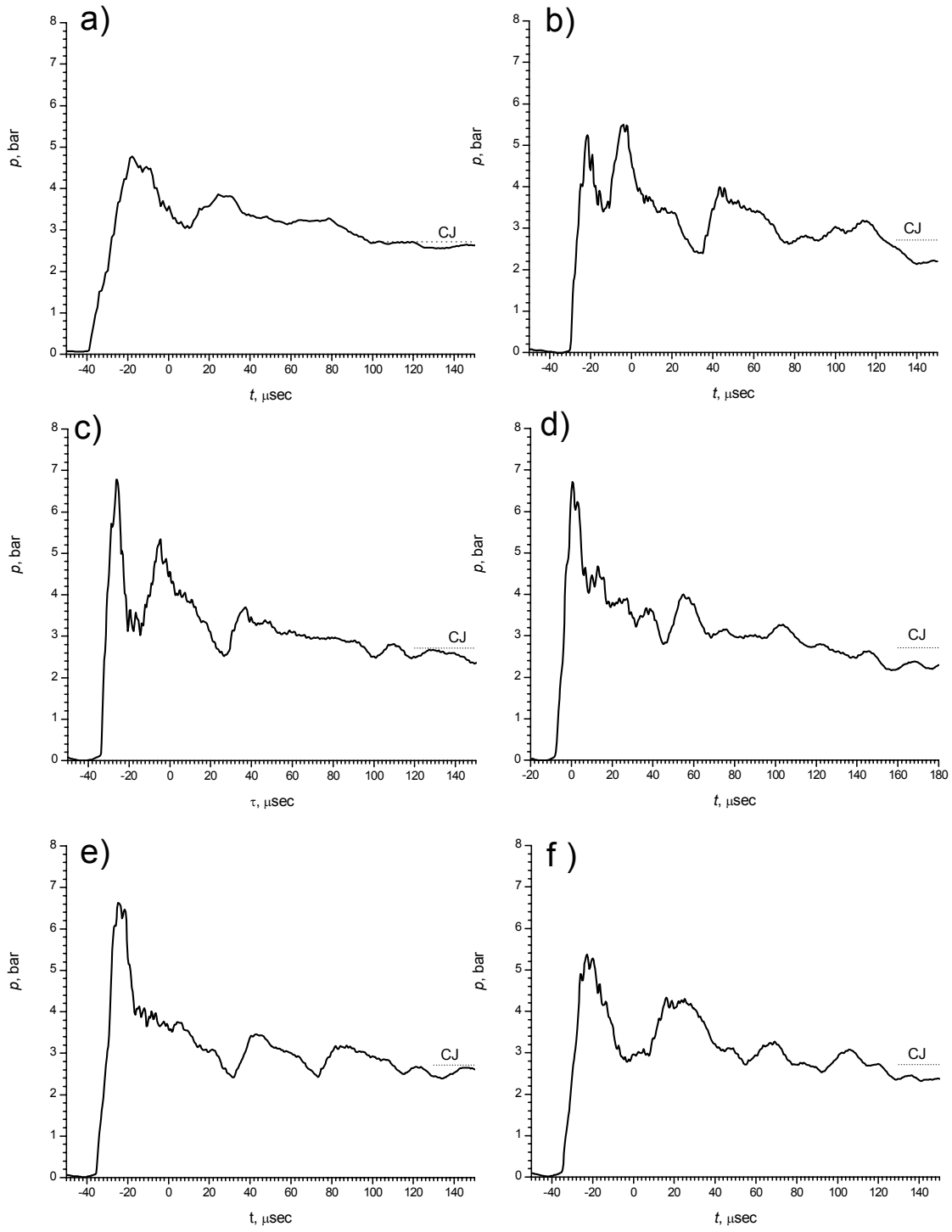

Figure 12 Pressure profiles obtained simultaneously as the photographs of Figure 11; time zero indicates the instant the photograph was taken

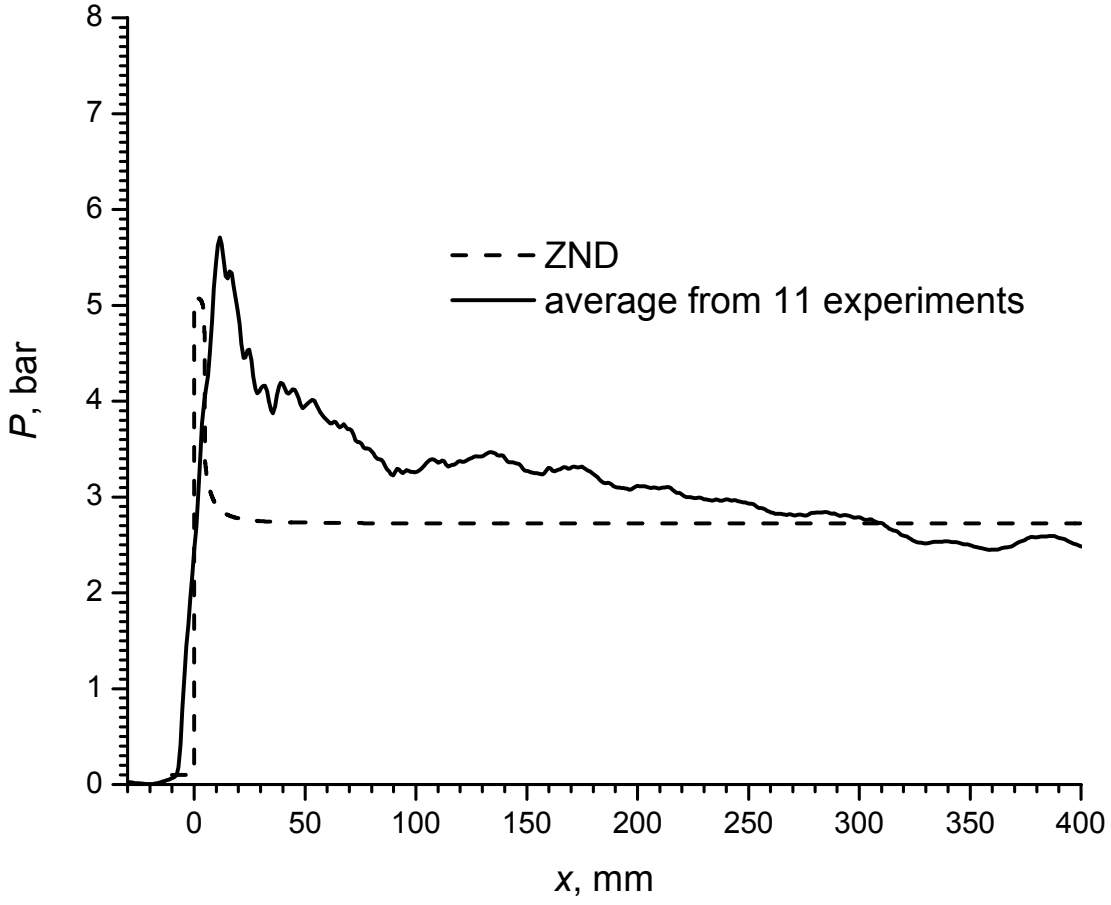

Figure 13 Average pressure profile obtained from 11 experiments and the ideal ZND pressure profile computed with the Lutz et al. (1988) kinetic mechanism

Figure 14

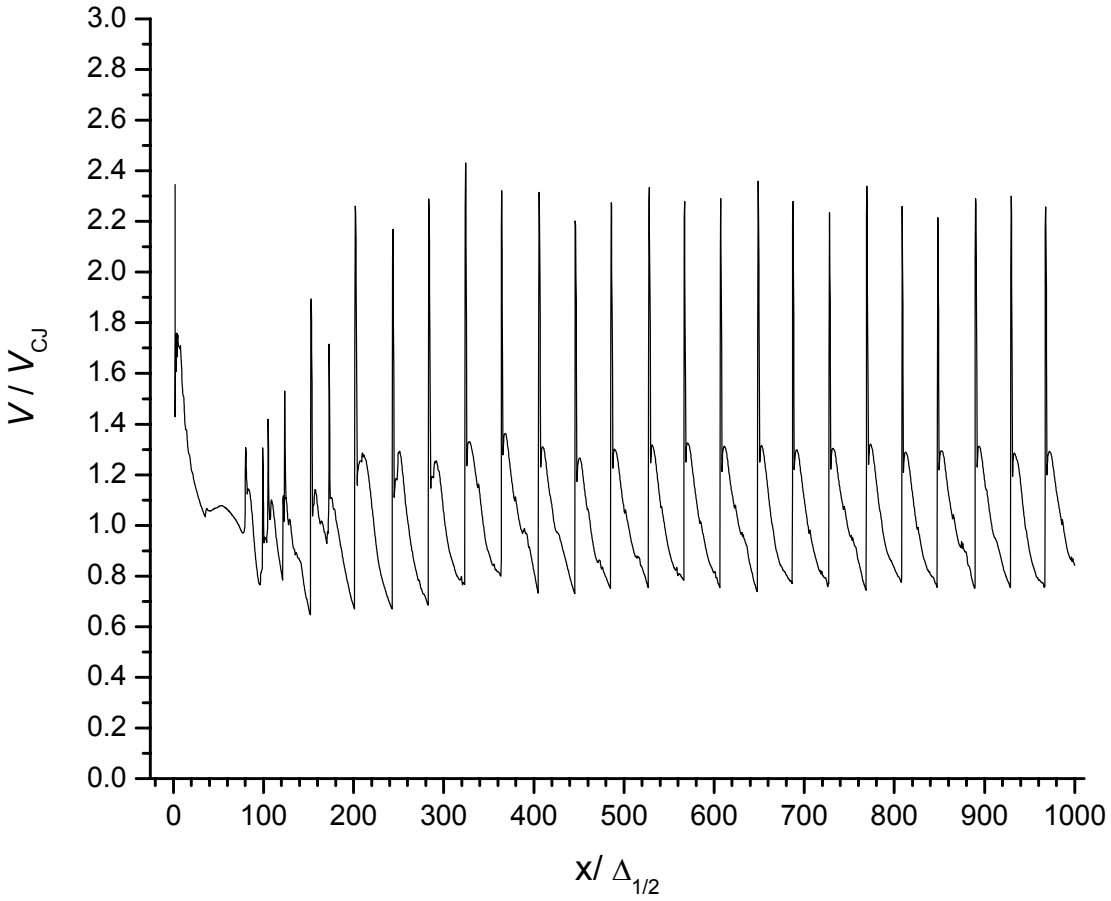

Figure 14 Velocity of the leading front recorded along the bottom wall of the computational domain for $E_a/RT_o = 27$

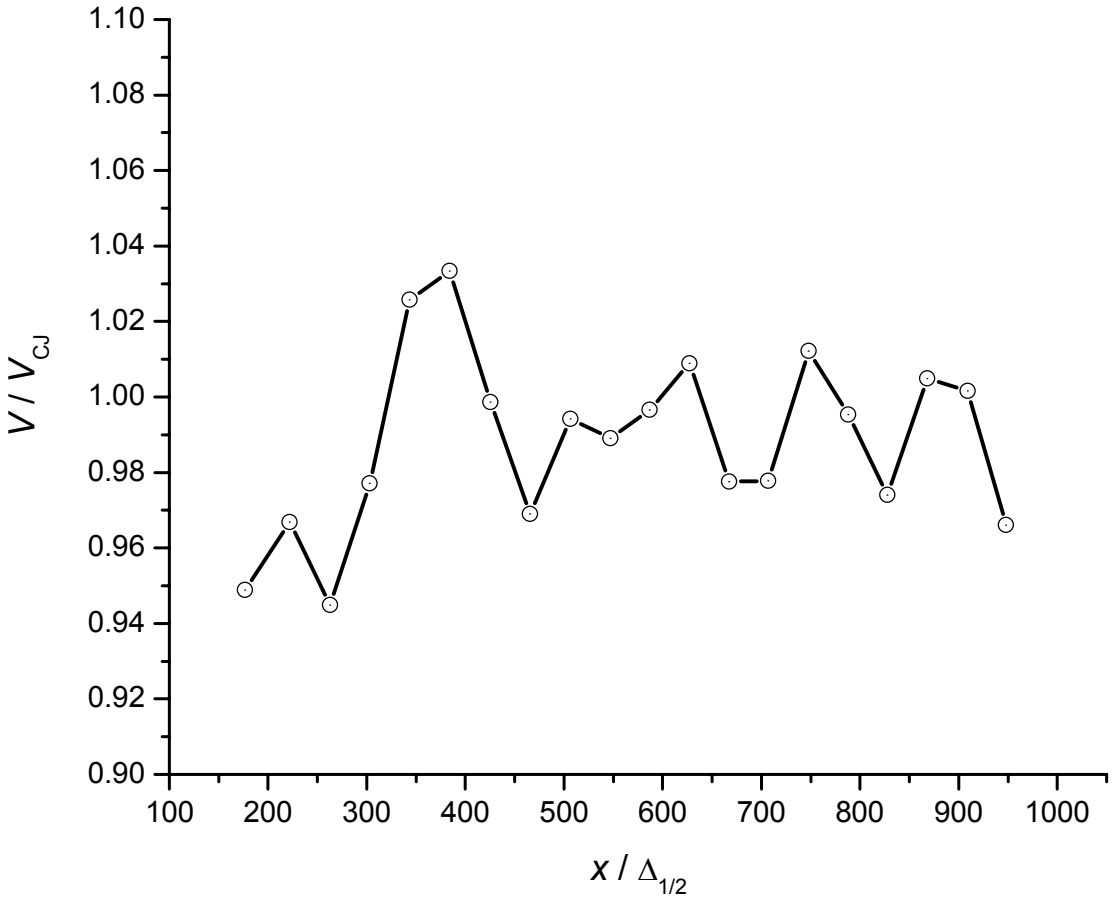

Figure 15 Cell-averaged velocity history of profile shown in Figure 14

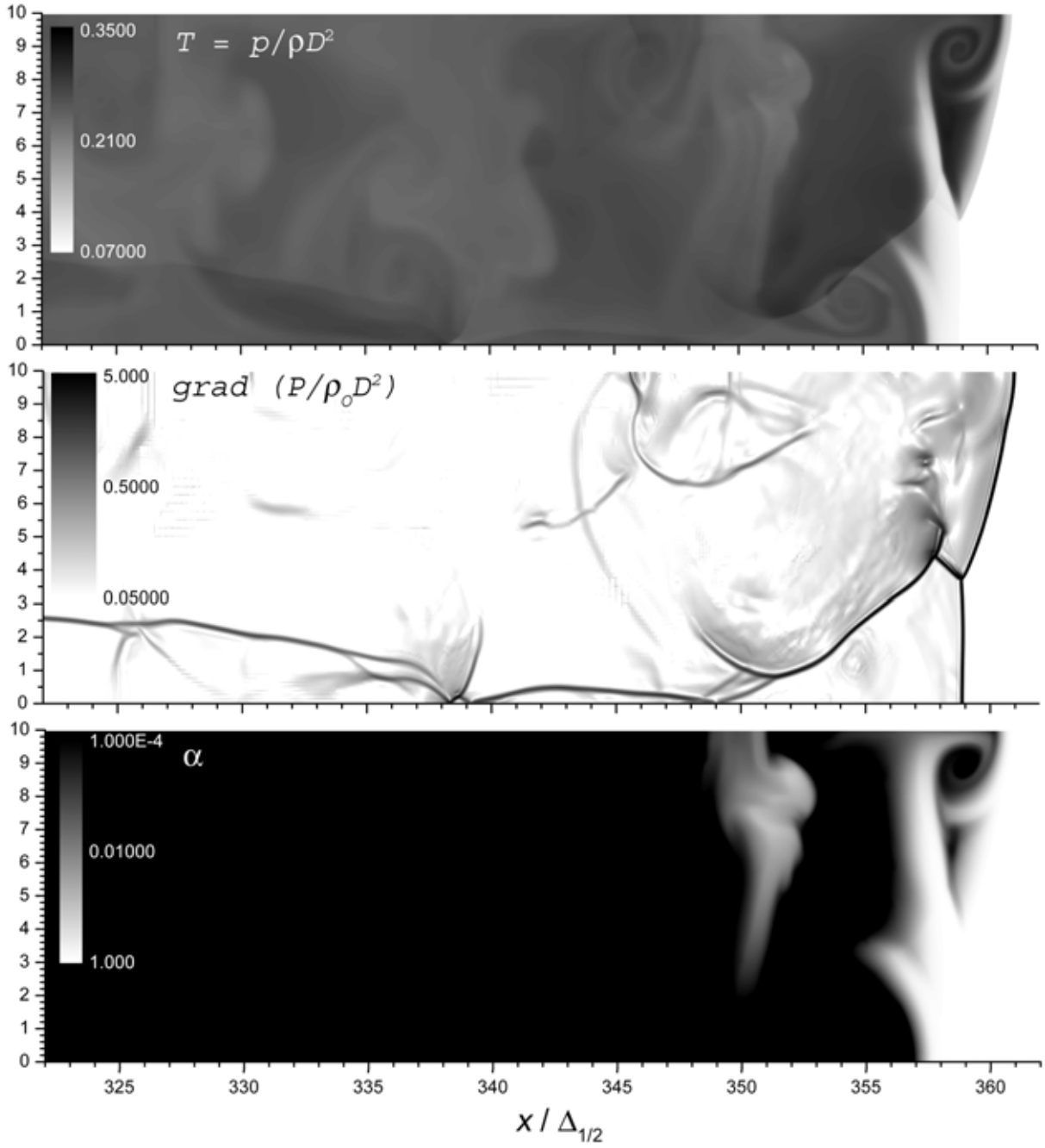

Figure 16 Temperature, pressure gradient and reaction progress variable for $E_a/RT_o = 27$

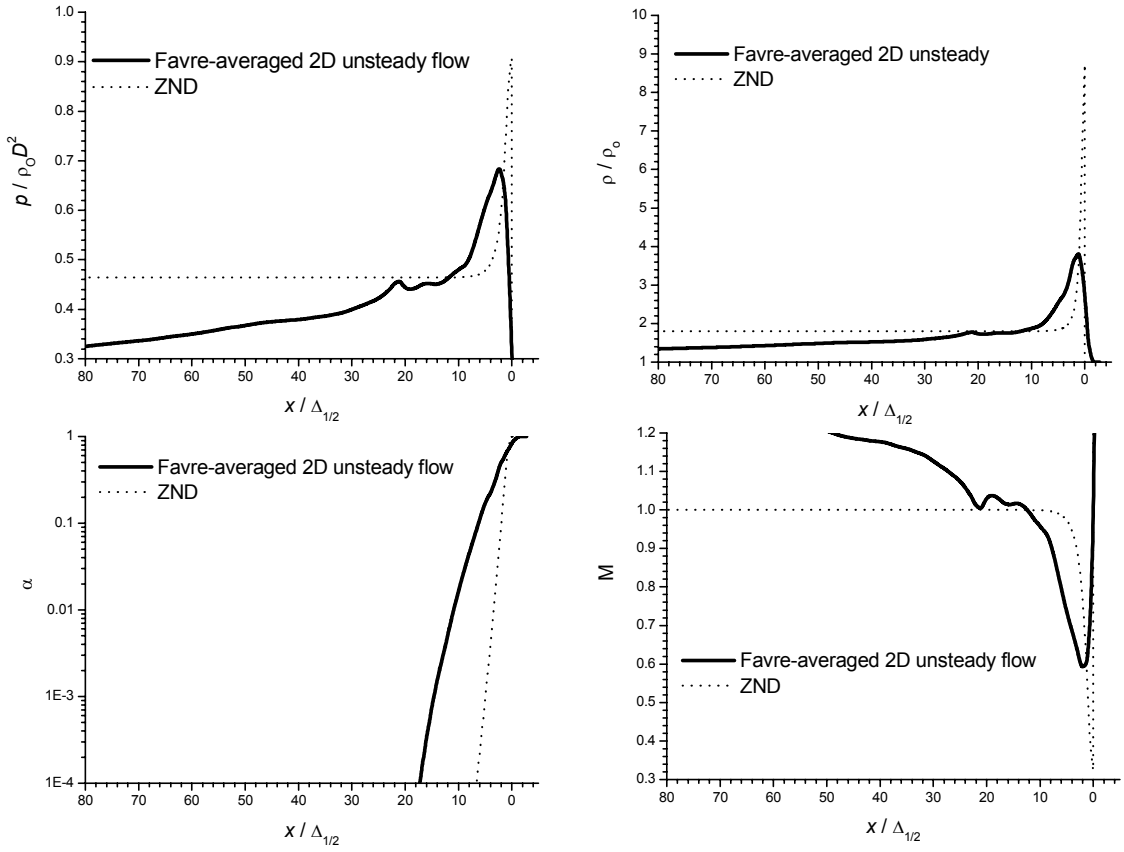

Figure 17 Favre-averaged profiles of pressure, density, reaction progress variable and Mach number for $E_a/RT_o = 27$

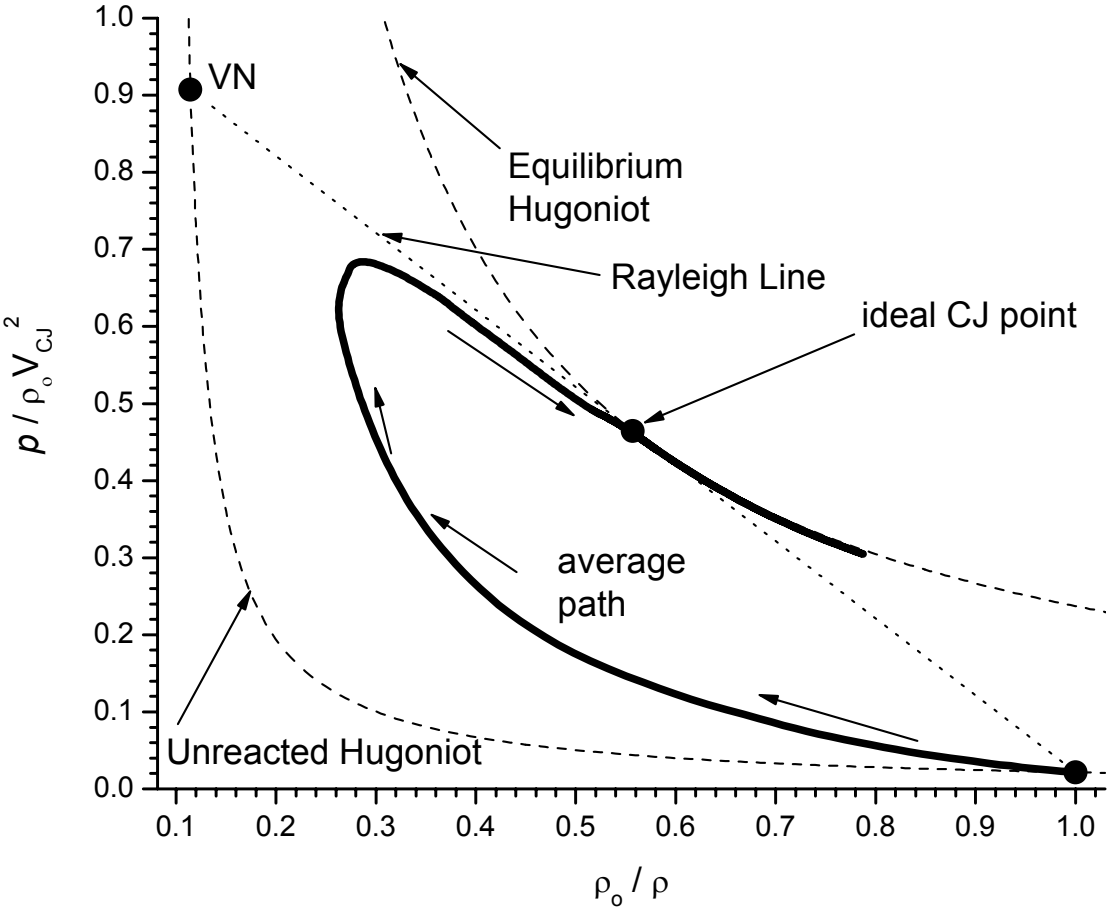

Figure 18 The integral curve of a mean Lagrangian particle traversing the detonation wave structure on a P-v diagram for $E_a/RT_o = 27$

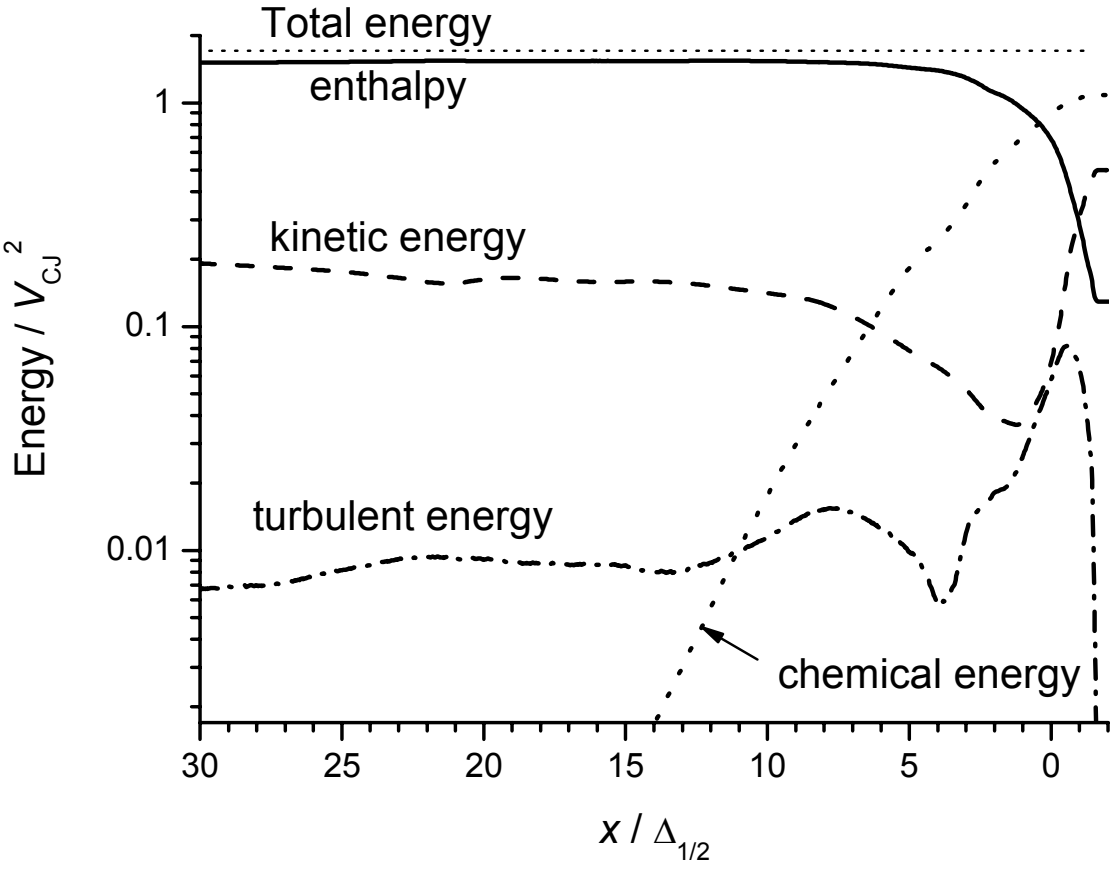

Figure 19 Energy partition for a mean fluid element traversing the detonation structure of the weakly unstable detonation

Figure 20

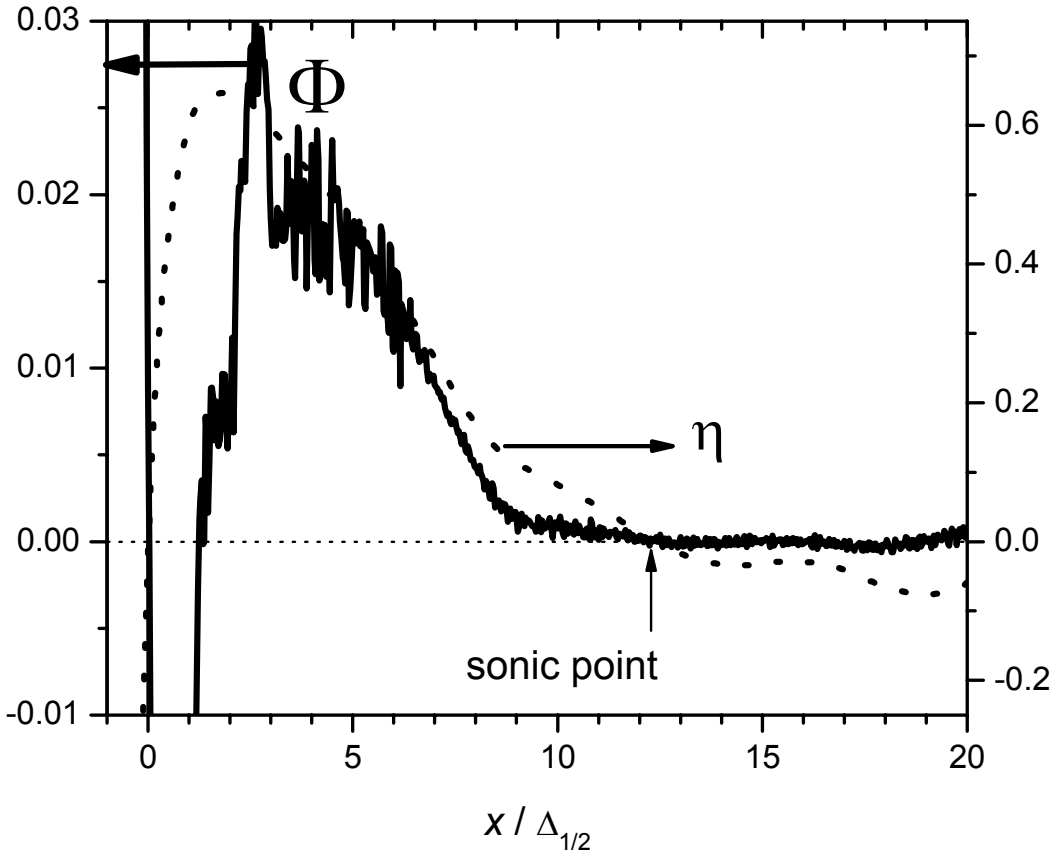

Figure 20 Variation of the thermicity Φ and sonicity η for $E_a/RT_o = 27$